Pb dispersion pathways in mountain soils contaminated by ancient mining and smelting activities

Floriane Guillevic, Magali Rossi, Anne-Lise Develle, Lorenzo Spadini, Jean M.F. Martins, Fabien Arnaud, Jérôme Poulenard

Pb dispersion pathways in mountain soils contaminated by ancient mining and smelting activities

Floriane Guillevic[1], Magali Rossi[1], Anne-Lise Develle[1], Lorenzo Spadini[2], Jean M.F. Martins[2] Fabien Arnaud[1], Jérôme Poulenard[1]

[1]Université Savoie Mont-Blanc, CNRS, EDYTEM, F-73000, Chambéry, France

[2]Université Grenoble Alpes, CNRS, G-INP, IRD, IGE, F-38000 Grenoble, France

Keywords

Mining and smelting soils, Pb-bearing phases, Pb-bearing Mn (hydr-)oxides, Pb mobilisation

Abstract

Over the last millennia, mining and smelting activities have produced large amounts of mine and metallurgical wastes that remain enriched in potentially toxic trace elements (PTE). A spatial distribution of Pb content was coupled to mineralogical observations and single extraction tests to characterise the Pb contamination legacy and Pb dispersion trajectories in an ancient mining and smelting site that has been abandoned for approximatively 200 years. In the Peisey-Nancroix Pb-Ag mine (Savoy, France), extreme anthropogenic Pb contamination is located close to the slag heaps and along ore and slag transport paths. The contamination gradient is restricted to a few hundred metres downhill, down to background Pb values. The Pb-bearing phases change along the contamination gradient. The most contaminated soils contain significant amounts of galena and slags that are more or less weathered into pyromorphite and cerussite. Pb-bearing Mn (hydr-)oxides are the most stable and ubiquitous forms of Pb, which proportions increase downgradient. Despite the presence of some stable Pb-bearing phases (pyromorphite, Pb-bearing Mn (hydr-)oxides), extraction tests indicate that a small proportion of Pb may still be mobile over time.

1. Introduction

Since the beginning of metallurgy, the exploitation of geological resources has been one of the most significant human activities releasing metals into the environment. Over the last millennia, mining and smelting activities have produced large amounts of mine wastes (waste dumps and tailings) and metallurgical wastes (slags and fumes) that remain enriched in potentially toxic trace elements (PTE; e.g., Pb, Sb, As, Cd, Cu and Zn). These wastes are sources of contamination, from which PTE are dispersed into the environment through different mechanisms. Ore smelting activities produce atmospheric particles carrying PTE over several tens of kilometres (Zdanowicz et al. 2006, Navel et al. 2015) to thousands of kilometres (Hong et al. 1994, Doucet and Carignan 2001, Cloquet et al. 2006, Cloquet et al. 2015). Old mining and metallurgical wastes are usually abandoned on soils without any protection and therefore are subjected to weathering. Particles of wastes can be transported by wind, gravity, runoff water or even by anthropogenic transport. Weathering of mining and metallurgical wastes may induce the transfer of PTE within runoff water and soils as free ions or complexes. Overall, these remobilisation processes lead to the release of PTE to the environment for centuries or even millennia after mining and smelting have ceased (e.g., Galuszka et al. 2015, Hansson et al. 2017, Camizuli et al. 2021), making the metal contamination legacy an environmental issue that requires attention in many places in the world (van der Voet et al. 2013). Among PTE, lead (Pb) is considered one of the most toxic elements in the environment (Alloway 2013). Its toxicity depends on its mobility and reactivity between abiotic compartments and biota (bioavailability). The soil is one of the environmental compartments most affected by mining and metallurgical wastes as it is the closest sink to the wastes. Very high metal contents in soils are often measured in the vicinity of former smelters and former mines (Ettler 2016, Cortada et al. 2018, Kříbek et al. 2019). Soil quality guidelines only consider metal content as a contamination criterion (e.g., Canadian Environmental Quality Guidelines (CEQGs) for soils:

Pb = 70 mg.kg^{-1}; United States Environmental Protection Agency (US EPA): Pb = 400 mg.kg^{-1}). However, metal speciation is the key parameter for assessing the mobility of metals and their biological harmfulness (Lejon et al. 2008, Navel et al. 2014, Spadini et al. 2018). Lead speciation is influenced by soil properties that tend to reduce its transfer (Alloway 2013), therefore, Pb is generally considered immobile.

To better limit the environmental impacts of future mining activities, it appears necessary to understand the long-term behaviour of PTE (dispersion and persistence) in the environment by developing studies on mining sites that have been abandoned for several hundred years.

Thousands of ore deposits have been formed and are located in mountain ranges. In the French Alps, hundreds of small ore deposits and occurrences have been reported by the French Geological Survey (BRGM). Environmental contamination related to past mining activities has already been identified in the French Alps based on records of direct atmospheric fallout deposition from mining exploitation in lake sediments (Arnaud et al. 2006, Elbaz-Poulichet et al. 2020) and remobilisation of abandoned mining and metallurgical wastes in river sediments (Camizuli et al. 2021). While recent studies showed the persistence of PTE contamination in former mining soils in the Vosges Mountains over hundreds of years (Monna et al. 2011, Mariet et al. 2017), this contamination has never been studied in alpine soils.

PTE contamination studies have often relied only on geochemical data such as PTE contents, which are insufficient to encompass their behaviours. Nevertheless, a combination of geochemical, mineralogical and extraction tests has more widely been used in PTE contamination studies (Swed et al. 2022, Chopin and Alloway 2007). However, the spatialisation of these data has rarely been undertaken and could help to better characterise the PTE dispersion from the sources of contamination to sinks. This paper aims to characterise the environmental legacy of former mining and smelting activities in the soils of a mountain mining site abandoned for more than 150 years: the Pb-Ag mine of Peisey-Nancroix, Savoy, France. A

spatial approach, coupling soil properties, geochemistry, mineralogical observations, and single extraction tests, allows us to discuss the mobility, transfer mechanisms and remobilisation of lead in soils for more than 150 years.

2. The Pb-Ag mine of Peisey-Nancroix (Savoy, France)

The northern French Alps have been mined for millennia (Judet 2014, Peloux et al. 2015), with the 18th and 19th century being the apex of industrial ore extraction in terms of production and number of sites. Indeed, most of these mines closed between the 19th and 20th centuries (Judet 2014) leaving hundreds of uncontrolled contamination spots in the environment. Pb, as a by-product of silver mining, was the most extracted nonferrous metal in France (Garçon 1995), providing large amounts of mining and smelting wastes that were abandoned all over the territory. The Peisey-Nancroix mining site has a former regional importance, and no anthropization has been identified since mine closure. The mining site is located in the northern French Alps at 1500 m a.s.l. on the Vanoise Massif, on the left bank of the Ponturin River (Figure 1). The mean annual temperature at the site is 1.5 °C and snow covers the area from November to May. The prevailing wind direction trends from northeast to southwest flowing up the valley. The ore deposit is located along the Internal Briançonnais Fault (IBF), which allows thrusting of the Internal Briançonnais on the External Briançonnais. The External Briançonnais is essentially composed of Carboniferous schists that extend over a few kilometres downstream from the mine site, overlying the Variscan basement. In the study area, the Internal Briançonnais is composed of various Variscan crystalline rocks (metagabbros, metabasites, micaschists and gneisses) and Permian micaschists. Some marbles of unknown age are also present in the area.

The Pb-Ag deposit of Peisey-Nancroix is hosted in Permian schists and Triassic quartzites of the External Briançonnais unit, which are trapped within the Internal Briançonnais Fault. The IBF is evidenced by the presence of Triassic dolomites that were brecciated and partly dissolved

during alpine thrusting, called cargneules. The ore consists mainly of galena (PbS) and pyrite (FeS) that are disseminated or concentrated in veinlets. Silver is hosted in As-rich tetrahedrite ($[Cu,Fe]_{12}Sb_4S_{13}$) that occurs as small inclusions within galena. Bertauts et al. (2022) provide a thorough description of the ore mineralogy. Galena and Ag-As-rich tetrahedrite were mined industrially between 1734 and 1866 to produce 22000 t Pb and 52 t Ag (Meloux, 1975). The ore was smelted on site for 90 years (1745-1824, Barbier 1875). The ore processing and metallurgical facilities were built on the edge of an alluvial cone that contains Variscan basement rocks and cargneules. A cargneule scree is intercalated in the alluvial cone on the western side of the mine site (Figure 1-B).

At the beginning of the exploitation, the ore was crushed, ground, and washed near the metallurgical and ore smelting site (O.S. site), immediately next to the mine entrance and the Arc stream (Figure 1-C). Soon, ore processing was moved further north to the ore-processing site (O.P. site) to take advantage of greater hydraulic power. A dewatering gallery allowed groundwater evacuation, aeration and ore transport directly to the O.P. site (Barbier 1875). The crushed ore was then transported from the ore-processing site to the ore-smelting site by a pathway that is still visible on the site. Close to the O.S. site, thousands of tons of abandoned waste rocks and smelting residues (slags) were stored and are still visible (Figure 1-C).

Figure 1 should be inserted here

3. Material and methods

3.1. Contamination source materials

Slags (n = 3) and waste rocks (n = 3) were sampled randomly on the heaps. Polished thin sections were made to perform scanning electron microscopy (SEM) observations to identify Pb-bearing phases. Each sample was analysed for major and trace elements by inductively coupled plasma- optical-emission-spectrometry (ICP-OES) and inductively coupled plasma-

mass-spectrometry (ICP-MS), respectively, at the Service d'Analyse des Roches et des Minéraux (France, Carignan et al. 2001).

3.2. Soil sampling

With the help of a manual auger, 117 topsoils (0-20 cm) were sampled on a 40x40 metre grid from the O.S site to the O.P site (Figure 2-B) to characterise the spatial distribution of the contamination. These soil samples were air-dried for several days, gently crushed and sieved to 2 mm. The coarse fraction (> 2 mm) was observed under a binocular microscope to study the translocation of ore (e.g., galena) and slag particles. The fine fraction (< 2 mm) was kept for further analysis as Pb-bearing phases tend to concentrate in the fine fraction. In addition, a distant topsoil from waste heaps was sampled 2 km upstream on the same alluvial cone (yellow pentagon on Figure 1-B).

3.3. Physical and chemical characterisation of soils

Soil properties play an important role in the mobility of Pb. Soil organic matter (SOM) and carbonate contents were assessed by loss-on-ignition (LOI) using a furnace for the whole soil dataset (n = 117). Weight loss after a 550 °C-first and 950 °C-second heating step corresponds to the SOM and carbonate (%) fractions, respectively (Heiri et al. 2001). Detailed analyses were performed on 27 soil samples at the French national reference soil laboratory (INRAE, France) including particle size distribution (5 fractions), pH (ISO 10390), cation exchange capacity (CEC), and exchangeable cation content (ISO 23470, cobaltihexamine method). The $SOM_{550°C}$ and $Carbonates_{950°C}$ fractions were compared to the measured equivalent $CaCO_3$ total content ($CaCO_{3T}$, ISO 10693, volumetric method), the C total content (C_T, ISO 10694, dry combustion), and the N total content (N_T, ISO 13878). The total organic carbon (TOC) and organic matter (OM) contents were calculated as follows :

$$(1)\ \mathrm{TOC} = \mathrm{C_T} - \left(\mathrm{CaCO_{3_T}} * 0.12\right)$$

$$(2)\ \mathrm{OM} = \mathrm{TOC} * 1.73$$

The calculation of an equivalent $CaCO_{3T}$ content by the volumetric method may be improper when dolomite is predominant (Vuong et al. 2016). However, a comparison of the LOI and dry combustion methods showed a good linear trend between $Carbonates_{950°C}$ and $CaCO_{3T}$ ($R^2 = 0.83$) and between $SOM_{550°C}$ and OM ($R^2 = 0.95$) assessments (Supplementary Material Table S1). The $Carbonates_{950°C}$ and $SOM_{550°C}$ content from the LOI measurements were then used in the following results as a good estimator for the whole soil dataset.

3.4. Quantitative analysis of soils by WDS-XRF

The total Pb content of the soils was assessed by measuring the chemical content with a Brucker S8 Tiger wavelength dispersive X-ray fluorescence spectrometer (WDS-XRF) equipped with a Rh anode X-ray tube (1 kW, 50 kV, and 170 mA). A mass of 7 g of the fine fraction of soil (< 2 mm) was crushed and pressed with 10 % Licowax C powder into 34-mm diameter pellets with a manual press (at 15 $kN.m^{-3}$). Aliquot duplicates of 12 soil samples were prepared and added to the sample list (Table S2). A certified standard was introduced at regular interval in the unknown samples list. The WDS-XRF calibration method included 12 standard samples, with 8 certified standards and 4 internal standards for very high Pb content (Pb content > 1000 $mg.kg^{-1}$, Table S3). The soil samples were analysed under vacuum conditions. The acquisition time of each spectrum was approximately 30 min for 23 elements. Hereafter, major elements (Na_2O, MgO, Al_2O_3, SiO_2, P_2O_5, K_2O, CaO, TiO_2, MnO, and Fe_2O_3) are given in weighted percentages (wt. %), and minor and trace elements (V, Cr, Co, Ni, Cu, Zn, As, Br, Rb, Zr, Ba, Pb, and Sb) in $mg.kg^{-1}$. Details of the method are available in Table S4.

The Pb Enrichment factor (EF_{Pb}) and Pb geoaccumulation index ($Igeo_{Pb}$) helping to discriminate anthropogenic from natural geogenic contamination were calculated (Chester and Stoner 1973, Müller 1979 and Reimann and de Caritat 2005). The EF_{Pb} was calculated

considering Ti as an immobile element with a content range close to Pb in contaminated soil (Thiombane 2019):

$$(3)\ EF = \frac{\left(\frac{M}{Ti}\right)_x}{\left(\frac{M}{Ti}\right)_{bkg}}$$

where M_x and Ti_x are the concentrations of the element and Ti in the soil sample, while M_{bkg} and Ti_{bkg} are their concentrations in the reference soil sample chosen as the local pedo-geochemical background. The enrichment factor was classified into 7 classes (Table S5). A common approach to estimate metal enrichment above background is to calculate the geoaccumulation index (Igeo) as proposed by Müller (1979). This index is calculated as follows:

$$(4)\ Igeo = log2(M\_x/(1.5 * M_{bkg}))$$

where M_x is the concentration of the element in enriched samples, and M_{bkg} is the background or pristine concentration of the element considered. The Factor 1.5 is introduced to minimise the effect of possible variations in the background values which may be attributed to lithological variations (Stoffers et al. 1986). Müller (1979) proposed 7 descriptive classes to assess the degree of metal pollution for increasing Igeo values (Table S5).

3.5. Mineralogical characterisation

Quantitative analysis of minerals from 10 soil samples (< 2 mm) was performed in the X-ray Diffractometry Laboratory of the Institut des Sciences de la Terre of Grenoble (ISTerre, France). X-Ray Diffraction (XRD) patterns were collected with a Bruker D5000 X-ray diffractometer equipped with a Sol-XE Si (Li) detector operated at 40 kV and 40 mA (Baltic Scientific Instruments). The Rietveld refinements of diffractograms obtained from disoriented powders of the bulk samples, were carried out with Profex software (Doebelin and Kleeberg

2015). The clay fraction analysis was used to refine the phyllosilicate description, and the diffractograms obtained were fit with Sybilla software (Aplin et al. 2006).

The Pb-bearing phases were identified for 19 soils using scanning electron microscopy (SEM) imaging and semiquantitative analyses at the ISTerre laboratory on an epoxy mounting pad and with free coated powders, with a Vega3 Tescan equipped with a 30 mm^2 X-Ray SDD detector (EDX). Detailed observations were carried out on a smaller scale (hundreds of nanometres to micrometres) using a SEM-field emission gun (FEG), JEOL IT500HR equipped with an energy dispersive X-ray spectrometer (EDX) at the Consortium des Moyens Technologiques Communs (CMTC Grenoble, France).

3.6. Single extraction tests

Single extraction tests are one of the few tools available to determine PTE mobilisation in soils related to metal speciation (Rao et al. 2008). Despite their inherent limitation, they permit us to generally evaluate the potential mobility (long-term) and the mobile fraction of Pb in soils (Quevauviller 1998, Gupta et al. 1996). Such tests were carried out on 21 samples selected according to their Pb content and soil properties. Three different extractants with increasing extraction power were used: distilled water, humic acid solution and an ethylene-diamine-tetra-acetic acid (EDTA) solution. Humic acids are used to mimic both degraded polymerized organic matter in soils (to which humic acids belong) and dissolved soil organic matter of soil, which are known to have a high density of reactivity sites similar to that of as humic acids (Causse et al. 2003).

A 2 g mass of soil (< 2 mm) mixed with 20 ml of extractant solution (solid:liquid ratio of 10) was agitated on a vibrating plate for 48 hours. Humic acid extraction was performed with a 0.1 $g.L^{-1}$ humic acid solution (Agros organic 50-60 %) and EDTA extraction was performed with a 10 $mmol.L^{-1}$ EDTA, 1 M Na-acetate solution yielding a buffering pH of 7 (AFNOR X31-

120). Each extraction was duplicated. Extracts were filtered at 0.45 µm and stabilised with 2 % HNO_3 before analysis by ICP-AES (Varian 720ES Atomic Emission Spectrometer, IGE, France). ICP-AES emission at 220,353 nm was used for determination of Pb. The limit of detection was 0.02 $mg.L^{-1}$ (L.O.D. = mean of blanks + 3σ) and the limit of quantification was 0.04 $mg.L^{-1}$ (L.O.Q. mean of blanks + 10σ). The mean of the Pb-extracted values for duplicates was calculated for each sample and used in the results. If a duplicate was below the L.O.Q, half of the L.O.D. was assigned to the sample. Samples were compared based on the percentage of Pb extracted (per extractant) as a function of the total Pb content, calculated for each sample:

$$(5)\ Part\ of\ extracted\ Pb\ (\%)\ = (extracted\ Pb)/(total\ Pb\ content) * 100$$

3.7. Analytical data treatment

Data analysis was carried out in R (open-source software, http://cran.r-project.org). Despite the constant sum problem of the compositional data of soil, basic statistics (minimum, percentiles, maximum, etc.) were calculated for an easier comparison with guidelines. Clr-transformation was then applied to the geochemical (major, traces and SOM content) dataset to perform statistical analysis of compositional data. Hierarchical classification following a principal component analysis (FactomineR) was performed to distinguish the different soil types in the study area.

All data (geochemistry, mineralogy, extraction tests, etc.) were reported on a GIS (ArcGiS) to develop a source-to-sink spatial analysis.

4. Results

4.1. Slags and waste rocks compositions

Table 1 provides geochemical compositions of some waste rocks and slags. The analysed waste rocks contain up to 7.1 wt. % for Pb, 125 $mg.kg^{-1}$ for Zn and 137 $mg.kg^{-1}$ for Sb. The PTE

contents of slags were higher than those of the waste rocks: up to 10.8 wt. % Pb, 5276 $mg.kg^{-1}$ Zn and 1638 $mg.kg^{-1}$ Sb.

The Pb-bearing phases observed in the waste rocks are those found in the ore (Bertauts et al., 2022): galena is largely dominant, and bournonite is locally observed. Because of weathering of the wastes, galena may slightly be altered into cerussite. In slags, three different Pb-bearing phases embedded in a Si-Fe-Ca-Ba-Al-rich silicate matrix were evidenced by SEM observations: (i) Pb-oxides, with different advancement in weathering processes, which had an ovoid shape of one to several hundred micrometres with a porous rim (Figure 2-B and Figure 2-C); (ii) millimetric Fe-sulphide containing lead (Figure 2-C); and (iii) prills that were micrometric to tens of micrometres (Figure 2-E). Trace amounts of Pb were also found in the vitreous silicate-rich matrix (Figure 2-B).

Figure 2 should be inserted here

Table 1 should be inserted here

4.2. Soil properties

4.2.1. Majors elements, carbonates, and soil organic matter content

Based on a principal component analysis (PCA), hierarchical clustering (Figure S1) on principle components was performed on clr-transformed major element (Na_2O, MgO, Al_2O_3, SiO_2, P_2O_5, K_2O, CaO, TiO_2, MnO, and Fe_2O_3) and soil organic matter ($SOM_{550°C}$) content datasets (Figure 3-A). Pb was added as an additional illustrative variable to explain the variability. The PCA allowed the identification of 3 clusters: highly Pb-contaminated cambisols (Cluster 1), carbonate-rich less-contaminated cambisols (Cluster 2) and carbonate-poor less-contaminated cambisols (Cluster 3). Basic statistics (minimum, 10^{th}, 25^{th}, 50^{th}, 75^{th}, 90^{th}, IQR, and maximum) for the 3 groups of soils are presented in Table 2. This classification reflects the local geology of the study site, leading to contrasting soil bedrocks (Figure 3-B). Carbonate-poor soils (CPS,

cluster 3) were developed on the Nant-Fesson alluvial cone (dark grey in Figure 1-B) and present a high SiO_2 content (min.-max.: 42-70 wt. %; median: 53 wt. %) and a low CaO content (min.-max.: 0.3-12 wt. %; median: 2 wt. %). Carbonate-rich soils (CRS, cluster 2) were developed on top of cargneule screes and led to a higher CaO content (min.-max.: 11-26 wt. %; median: 17 wt. %). Highly contaminated soils (HCS, cluster 1) were located at the O.P. site (Samples O1 and Q1), the O.S. site (e.g., Samples D1 and B1), along the former ore transport paths (Sample F3), and a potential waste material storage area (Sample H7; Figure 3-B). Among these samples, sample D1, which was collected on a poorly vegetated slag heap, can be considered as a technosol essentially made of slags. Most of these HCS are chemically close to CRS. Hence, the hayfields exploited downwards from the waste heaps are divided into two chemically different soils: CRS to the west and CPS to the east of the site (Figure 3-B).

Figure 3 should be inserted here

Irrespective of the type of land-use (hayfields or forest cover), the soil organic matter ($SOM_{550°C}$) content in the CRS (min.-max.: 4-55 wt. %; median : 17 wt. %, Table 2 and Table S1) was twice as high as that in the CPS (min.-max.: 1-19 wt. %; median: 9 wt. %). Detailed analyses were performed on selected soil samples (n = 27, Table S6). A slightly higher pH was observed for the CRS (pH = 7.7) compared to the CPS (pH = 7.0), due to a higher $CaCO_{3T}$ content. The particle size distribution was similar for all soil samples. The clay fraction represented a minor fraction for all types of soils, with a content ranging from 5 to 16 %. The content of exchangeable cations was dominated by Ca and Mg (Ca = 11.3-32.7 $cmol+.kg^{-1}$, Mg = 0.6-6.7 $cmol+.kg^{-1}$).

Table 2 should be inserted here

4.2.2. Mineralogy of soils

According to XRD measurements carried out on the fine fraction (n = 10), the CRS was dominated by dolomite while the CPS was dominated by quartz, plagioclase, and clay minerals such as K-micas and expanding phyllosilicates (Table S7 and Figure S2). The only oxide identified was haematite, and its proportion contributed to less than 0.5 % to the total mineral content. With the exception of Sample P2, which was located on the right bank of the Nant Fesson stream, all samples were abundant in amorphous phases ranging from 2 % to 30 % in the soils. This amorphous material most likely corresponds to slag fragments, organic matter, or coal.

4.3. Pb contamination of soils

4.3.1. Definition of the local pedo-geochemical soil background

To define a reference of Pb in soil, several options were considered: i) an external reference (continental crust content), ii) the average Pb content of the rocks in the watershed (excluding mineralized rocks), iii) a deep-horizon soil (45-60 cm) sampled the farthest away from the O.S. site, near the Ponturin River (sampled between Samples K5 and L6; Figure 3-B), and iv) a distant soil (0-20 cm) located 2 km upwards on the same alluvial cone, which was sampled near the active torrent in order to have the youngest possible soil to avoid the presence of airborne Pb emitted during smelting. The two soils (deep-horizon soil and distant soil) had a Pb content one order of magnitude larger than that of the middle continental crust and the local lithologies (Table 3). The distant soil from the alluvial cone was selected as a reference, considering (i) that the comparison of rocks and soils may not be relevant, and (ii) that a deep-horizon soil near the mine site could be naturally contaminated by the presence of the ore deposit.

Table 3 should be inserted here.

4.3.2. Total Pb content of soils

Geochemical maps based on PTE content allow the identification of "hot spots" of contamination (Rao et al. 2008). Among the PTE analysed (Table 2), Pb had the highest values above the guidelines and references (Table 3). The Pb content varied from < 10 $mg.kg^{-1}$ to 3.8 wt. % (median: 1173 $mg.kg^{-1}$). The high contents of Cu, Zn and Sb were very localised to the O.S. and O.P. sites. Therefore, the following study focuses on the Pb distribution. The highest Pb content was measured in the soils from the O.S. site and along the edge of the forest and hayfield (Figure 4-A). Downwards from the hayfield slope, the Pb content decreased down to the local pedo-geochemical background (blue points in Figure 4-A). The spatial distribution of Pb content in soils indicated a clear gradient of anthropogenic contamination from the mine site downwards. Major element and other trace element contents are available in Supplementary Material Table S8.

Figure 4 should be inserted here.

4.3.3. Enrichment factor & geoaccumulation index

In comparison to the reference soil content, extreme enrichment (EF_{Pb} >> 50 and up to 250) and extreme contamination were observed near the O.S. and O.P. sites, and between the two sites along transport paths (Figure 4-B). There was a rapid decrease in EF_{Pb} and $Igeo_{Pb}$ down to a minor to moderate enrichment and contamination, respectively (EF < 5 and Igeo < 2; Figure 4-B and 4-C). No enrichment and contamination were observed in the samples on the right bank of the Nant Fesson and in the samples the closest to the Ponturin River.

4.3.4. Pb association with major elements

Overall, the Pb content of the soil had a medium correlation with MnO ($r^2 = 0.58$, $p < 0.001$; Table 4) and P_2O_5 ($r^2 = 0.57$, $p < 0.001$). In detail, carbonate-rich soils (CRS) had a significantly higher correlation between Pb and MnO than highly contaminated and carbonate-poor soils (HCS and CPS, respectively). Nevertheless, the HCS and the CRS had a higher average

correlation between Pb and P_2O_5 than CPS. These correlations suggest that Pb in the CRS was mainly associated with Mn first and P then, whereas it was mostly associated with P in the HCS. In CPS, no strong correlation between Pb and any major element was observed. The distribution of Pb correlated well with the distribution of Sb ($r^2 = 0.79$, $p < 0.001$), especially for CRS and CPS, and with SOM ($r^2 = 0.43$, $p < 0.001$).

Table 4 should be inserted here

4.4. Pb-bearing phases in soils

The mineralogical nature of the Pb-bearing phases was investigated by (i) observation of the coarse fraction using a binocular microscope (> 2 mm, n = 117) to qualify the presence of slag or ore mineral particles (e.g., galena) and (ii) detailed observations on 19 fine fraction samples (free powder or pressed pellets) using SEM.

Coarse fraction (> 2 mm)

Qualitative binocular observations on the coarse fraction (small circles in Figure 5-A) showed the presence of slag particles in the soils in the vicinity of the O.S. site and along the ore transport pathways. This observation was confirmed by the presence of slag particles in the fine fraction (large circles in Figure 5-A). Fewer slag particles were observed downwards in the coarse fraction, suggesting a lower proportion or the absence of them in the fine fraction.

Figure 5 should be inserted here

Fine fraction (< 2 mm)

SEM observations allowed the identification of many phases that were not identified by XRD because they were not abundant enough (< 0.1 %). The Pb-bearing phases observed by SEM and their spatial distribution in the fine fraction of soils are shown in Figure 2 and Figure 5, respectively. Typical EDS spectra are presented in Figure S3 in the supplementary material.

Galena particles were observed only in the soils sampled in the vicinity of the waste heaps or along the former transport path between the O.S. and O.P. sites (Figure 5-A). They most likely fell from the heaps by gravity or due to human transport from the O.P. site to the O.S. site for smelting. SEM observations indicated a widespread distribution of Pb-rich slags and a restricted dispersion of galena (Figure 5-A), in agreement with qualitative observations on the coarse fraction. This result indicates that slag particles were the first primary contamination sources of PTE in soils.

Most of the galena particles in the soils have been weathered to a secondary reprecipitated mineral (Figure 2-D). The pseudomorphosis of galena to cerussite, called cerussite I, is recognisable by its tens of micrometres size and its preserved shape of vuggy-faced galena (Figure 2-D and Figure 2-F). Cerussite I was observed in the most Pb-contaminated soils. The vuggy aspect of these large cerussite particles was evidenced by ongoing alteration and dissolution of Pb, which may be partly transported in solution. Cerussite has also been observed in less contaminated samples (Figure 5-B). This cerussite II was not well crystallised and had a smaller-size and a filamentous structure, suggesting a leaching-reprecipitation mechanism (Figure 2-G). Cerussite was the only Pb-bearing mineral identified by XRD (< 0.1 %); it was only identified in three samples located at the O.S. site or along the ore transport pathway between the O.S. and O.P. sites (Table S7). Slag fragments were also often associated with cerussite at their edges.

In addition to cerussite II, Ca-rich pyromorphite ($Pb_5(PO_4)_3(Cl, OH, F)$) was observed at the O.S. site or along the former transport path (Figure 5-B), either as tens of micrometres-sized fibrous shapes or as micrometric rounded grains (Figure 2-J and Figure 2-K).

The most ubiquitous Pb-bearing phases were the Pb-bearing Mn (hydr-)oxides (Figure 5-B). Pb can either be adsorbed at the surface of the Mn (hydr-)oxides or included in the crystal lattice to form Pb-Mn (hydr-)oxides through $Pb^{2+} \Leftrightarrow Mn^{2+}$ substitution. SEM spectra and

semiquantitative analysis (Figure S3) indicated that the Pb stoichiometric part in the total phases is commonly several tens of percents. Such high Pb content suggest the occurrence of $Pb^{2+} \Leftrightarrow Mn^{2+}$ substitution rather than Pb-adsorption. A significant consistent C peak was associated with Pb-bearing Mn (hydr-)oxides in EDX analyses, suggesting an association of these (hydr-)oxides with carbonates and/or organic matter. Downwards from the slope, mineralogical observations tended to indicate a higher occurrence of rounded micrometric to tens of micrometres-sized aggregates of Pb-bearing Mn (hydr-)oxides (Figure 2-H and Figure 2-I) at the expense of Pb-bearing slags and galena particles. A minor proportion of Pb-bearing Fe-Mn (hydr-)oxides and Fe (hydr-)oxides with traces of Pb were also observed. Such Fe-rich phases likely derived from the alteration of pyrite.

Due to SEM-EDX detection limits and the very small amount of Pb adsorbed, it was very difficult to identify sorbed phases using SEM. However, Pb associated with clays and organic matter could occasionally be identified (Figure 5-B), based on the presence of a fairly small Pb peak observed in the SEM-EDX spectra (Figure S3). Because of its very low content, Pb is likely adsorbed on these phases.

4.5. Pb single extraction tests

The amount of Pb extracted by distilled water, humic acid and EDTA versus the total Pb content of the soil measured by WDS-XRF is shown in Figure 6. The total Pb content of soils and Pb-extracted by water, humic acid and EDTA showed a good linear trend (respectively $r^2 = 0.93$, $r^2 = 0.75$, and $r^2 = 0.91$, respectively). The higher the total Pb content of the soil was, the higher the amount of Pb extracted. Samples with a low Pb content extracted less Pb than highly contaminated samples in proportion to the total Pb content. This was visually observable because the three overall slopes established by the amount of Pb extracted from water, humic acid, and EDTA were steeper than the slope established by the total Pb content (Figure 6). Therefore, the percentage of extracted Pb relative to the total Pb content (see Equation 5) is

presented in Figure 7 to spatially visualise the distribution of extracted Pb fraction. Water-extracted Pb quantities from 5 samples and humic acid-extracted Pb quantities from 3 samples were below the detection limit (Table S9).

Figure 6 should be inserted here

4.5.1. Water extraction

The measurable water-extracted Pb quantities varied from 0.1 to 42 mg Pb kg^{-1}. The highly contaminated soil E3 had the highest extracted Pb content, followed by the highly contaminated soils B2A and D3 (downhill slag heap), which also presented very high water soluble Pb contents of 40 and 35 mg Pb kg^{-1}, respectively. The water-extracted Pb represented 0.02 to 0.25 % of the total Pb content of the soil samples (Figure 7)

Figure 7 should be inserted here.

4.5.2. Humic acid extraction

The measurable humic acid-extracted Pb quantities varied from 0.1 to 197 mg Pb kg^{-1}. The highly contaminated soil B2A had the highest Pb content of humic acid-extracted Pb. Humic acid-extracted Pb quantities were 2 to 5 times higher than water-extracted Pb quantities (Figure 6). Pb extracted by humic acid represented 0.02 to 1 % of the total Pb content of the soil samples (Figure 7).

4.5.3. EDTA extraction

EDTA-extracted Pb quantities were much higher, varying from 45 to 25 423 mg Pb kg^{-1}. They were equivalent to the total Pb content of most of the highly contaminated samples (Figure 6), with the exception of the most contaminated soil D3, which contains the most slag and coal

particles and therefore less accessible Pb. Pb extracted by EDTA represented 49 to 120 % of the total Pb content of the soil samples (Table S9). EDTA extractant is known to often leach a higher Pb content than the total Pb content (Sterckeman et al. 1996). These samples were fixed at 100 % in Figure 7 (Samples G3, G5, L2 and O1).

4.5.4. Data comparison

The soil samples were divided into 3 groups according to the total Pb content, the amount of Pb extracted by water and EDTA and the distance to the slag heaps (Table 5). The Group 1 samples had no or low Pb contamination (blue circles in Figure 7). They were characterised by a nonquantifiable water extraction of Pb and a low EDTA extraction of Pb (< 60 %). These samples were disconnected from the waste heaps downslope (H11; K9; and G8) or upstream of the ore transport pathway (K1). The Group 2 samples were moderately contaminated with Pb and characterised by low water extraction of Pb and median EDTA extraction of Pb (yellow circle in Figure 7). These samples were far away from mining and metallurgical wastes. The Group 3 samples were highly contaminated and characterised by high Pb water extraction and high Pb EDTA extraction (red circle in Figure 7). These samples were close to or in the immediate vicinity of mining and metallurgical wastes.

Table 5 should be inserted here

5. Discussion

Geochemical analyses provide evidence of extreme Pb contamination in the soils that is restricted to the ancient mining and smelting site of Peisey-Nancroix. The most contaminated soils are localised along anthropogenic features, close to the slag heaps and along the transport

pathway and dewatering gallery that connect the O.P. site to the O.S. site. Such a spatial distribution provides evidence of the anthropogenic origin of the contamination there.

5.1. Remobilisation and long-term mobility of Pb

5.1.1. Mobility of Pb

Water is considered to be a weak acid extractant that allows the determination of the water-soluble metal fraction, considered the most mobile fraction (Rao et al. 2008). No water-extractable Pb fraction was measured in the samples of extraction Group 1 (Figure 7), which corresponds to control samples due to their disconnection from the sources of contamination (slag heaps and transport pathways). Such a low Pb mobility suggests the absence of water-soluble phases, which corroborates the presence of only Pb-bearing Mn and Fe (hydr-)oxides in these samples (Figure 5-B). In contrast, the most contaminated soils in Group 3 samples had a high amount of water-extracted Pb, which still represents a small proportion of the total Pb content (Figure 7). Pb water-extracted quantities tended to decrease in soils downgradient and represented a smaller extracted fraction of the total Pb content (Group 2 samples).

The water-soluble fraction was generally defined as easily exchangeable Pb and bound to carbonates and/or organic matter (Sahuquillo et al. 2003). Cerussite was the most abundant Pb-bearing mineral in the highly contaminated samples, with slag particles (by relative proportion and by preferential weathering phase of galena and PbO in slags, Figure 5). Cerussite is known to be insoluble in pure water at neutral to alkaline pH (Keim and Markl 2015). However, one can consider the soil organic matter as a competitive ligand to cerussite conducting to Pb partial extraction in solution, under in-situ conditions. Water extraction tends also to leach the not easily observable Pb adsorbed phases, which is suggested by the good correlation between TOC and water Pb extracted ($r = 0.63$, $p < 0.05$, Table 6).

Table 6 should be inserted here.

The decrease in Pb mobility is associated with a decrease in Pb contamination in the soils, reflecting a redistribution of the Pb-bearing phases.

5.1.2. Potentially mobilisable Pb

EDTA is a strong complexing agent that acts as a metal extractant. It is often used to estimate the potentially mobilisable pool of metals (Cappuyns 2012) bound to soil organic matter (SOM) and carbonate complexes. EDTA-extraction tests of Group 1 samples showed the smallest fraction of Pb extracted by EDTA of all samples tested. Group 1 samples were uncontaminated or minimally contaminated, with less than 100 $mg.kg^{-1}$ Pb, which is insignificant in the long-term. In contrast, the samples in Group 3 had an EDTA-extracted Pb content between 80 to 100 % of the total Pb content. This result suggests that the Pb content of the Pb-bearing phases is mobilisable in the long-term and represents a potential source of Pb in soil solution. However, the EDTA-extractable Pb fraction decreased rapidly downgradient indicating a greater proportion of less mobilisable Pb-bearing minerals downgradient (Group 2 Samples M5 and K5; Figure 7). Ostergren et al. (1999) showed that EDTA successfully dissolved strongly bound surface Pb complexes and EDTA-soluble phases as carbonates and poorly crystalline Fe (hydr-)oxides.

There was an evolution of the chemical form of Pb from waste heaps to downgradient: Pb water soluble forms (weakly bound) disappeared for the benefit of a higher proportion of more stable phases (Pb-bearing Mn (hydr-)oxides), leading to a less mobile Pb down the slope. However, EDTA extraction tests suggest that an important pool of Pb, stocked in the most stable phases, could be mobilised in the long-term.

5.2. Pb dispersion processes in soils

Two Pb dispersion processes were identified by combining mineralogical observations, geochemical contents and leaching tests: particulate translocation of the Pb-bearing primary

contamination phases and Pb leaching of the primary contamination phases leading to reprecipitated or adsorbed Pb.

5.2.1. Translocation of particles

The most contaminated soils provided evidence of the presence of significant amounts of galena and slag particles, which are weathered in soils. A few dropped galena were identified in the fine fraction of highly contaminated soils and in soils along former transport paths. No coarse (> 2 mm) or fine (< 2 mm) galena particles were observed in soils down to the O.S. site. In contrast, slag particles were more widespread in the coarse and fine fractions of soils. Nevertheless, qualitative mineralogical observations indicated their scarcer proportion downwards in both the fine fraction and coarse fractions.

The extensive dispersion of slags can be explained by the natural translocation of small slag particles, by the reuse of slags for roasting the ore and the reuse of slags for construction (path, roads, etc.). Particulate translocation of Pb-bearing slag fragments significantly contributed to the Pb contamination in the soils due to their high Pb content (several wt. %).

5.2.2. Leaching processes

5.2.2.1. Leaching-reprecipitation processes

The dispersion and weathering of Pb-bearing galena particles or slag phases in soils represents a source of Pb, which can be leached and reprecipitated. These primary Pb-bearing phases were transformed into secondary Pb-bearing reprecipitated phases: cerussite, pyromorphite and Pb-bearing Mn (hydr-)oxides.

Cerussite I was mainly observed in the most contaminated samples, located along the transport path and the dewatering gallery, between the O.S and O.P. sites. Galena particles are directly altered into cerussite (cerussite I) in carbonate-rich alkaline environments (Bao 2021), which is consistent with our observations. Cerussite I has a porous layer on its faces that accelerates

galena dissolution and releases Pb^{2+} into the pore waters (Lara et al. 2011). The released Pb^{2+} is likely to be reprecipitated further into cerussite II.

The restricted presence of Ca-rich pyromorphite in highly contaminated soils supports the significant correlation between Pb and P in these soils (Table 4). Pyromorphite is commonly observed in Pb-contaminated soils (Cotter-Howells and Thornton, 1991). It is considered a long-term host for Pb or a mature alteration product of Pb (Davies et al. 1993) and as the most insoluble secondary form of Pb in soils under a wide range of environmental conditions (Morin et al. 2001, Hettiarchchi et al. 2000, Nriagu et al. 1974). The substitution of Ca^{2+} for Pb^{2+} accentuates the insoluble character of pyromorphite (solid solution, Cotter-Howells 1994). Therefore, the Ca-rich pyromorphite observed at the site is considered to be highly insoluble (Figure S2). The source of P must be very localised within the highly contaminated soils as no pyromorphite was observed in the hayfields despite fertiliser application. The presence of monazite, xenotime and apatite in the ore (Bertauts et al. 2022) may be the main source of phosphorus as well as the P-enriched slags (Table 1). It can be assumed that pyromorphite crystallises as long as Pb is leached out and P is available (Buatier et al. 2001).

Pb-bearing Mn (hydr-)oxides, based on mineralogical observations, were the most ubiquitous Pb-bearing phases observed in soils and the dominant Pb-bearing phase observed downgradient. Mineralogical observations tended to show a decrease in cerussite and pyromorphite downgradient in favour of a greater proportion of Pb-bearing Mn (hydr-)oxides. It is widely known that Mn-(hydr-)oxides and Fe-(hydr-)oxides have a high capacity to retain PTE in the environment and are considered also as a mature alteration phase (Davis et al. 1993). The characteristics of the Pb-bearing Mn (hydr-)oxides suggest leaching of the Pb-bearing slag or galena particles, solute transport and reprecipitation.

5.2.2.2. Leaching-adsorption processes

Few Pb-adsorbed phases were observed knowing the limits of the SEM to identify such phases with a low to a very low Pb content using backscattered electrons. The observed spatial distribution of Pb-adsorbed on clays and organic matter (Figure 5-B) is likely not representative of their real distribution because of the high difficulty to identify these phases using SEM. Despite this difficulty, these phases play an important role in the mobility of Pb, as they can represent up to 50 % of the Pb-bearing phases in mining and smelting areas (Brown et al. 2009).

5.3. The airborne portion of the Pb contamination

Pb-rich atmospheric fallout was most likely been deposited on site during smelting. However, no Pb enrichment was evidenced among the farthest samples from the O.S. and O.P. sites (Figure 4-A), suggesting that the part of airborne lead contamination was negligible. Considering that smelter fumes can be transported over several kilometres to thousands of kilometres (Hong et al. 1994, Doucet and Carignan 2001, Cloquet et al. 2006, Zdanowicz et al. 2006; Cloquet et al. 2015), it is necessary to obtain samples from a few kilometres downwind to characterise airborne Pb contamination. Lake sediment cores were sampled in La Plagne Lake (7 km upstream of the mining site) together with soils from its watershed in order to quantify the contamination contribution of the atmospheric deposition to the total Pb contamination observed at the site in soils (Guillevic et al. in prep.).

6. Conclusion

This study shows the persistence of a 200 years Pb contamination in the vicinity of the Peisey-Nancroix Pb-Ag mine (Savoy, France). Severe anthropogenic Pb contamination is localised in soils around the former mining and smelting sites: it is restricted to anthropogenic features (slag heaps, former transport path and dewatering gallery) and decreases rapidly, in a few hundreds of metres in soils downwards. Slag particles are most likely the main source of Pb

contamination, especially particles dispersed by anthropogenic transport between the O.P and O.S sites.

Coupling mineralogical observations and extraction tests suggests a rearrangement of Pb-bearing phases from labile to more stable phases downgradient. The highest contaminated soils account for a higher proportion of water-soluble and less stable Pb-bearing phases, as Pb-carbonates and Pb-adsorbed phases tend to decrease downgradient for the benefit of a higher proportion of Pb-bearing Mn (hydr-)oxides which are more stable. A form of Pb stabilisation is set up by moving away from the sources of contamination. This study contributes to a better understanding of the long-term dispersion of Pb due to mining activities. Evaluation of the mining legacy in soils and its memory effects should involve mineralogical characterisation in addition to leaching tests, in order to assess the Pb mobility/stability. Such knowledge is necessary to establish mitigation strategies that limit PTE migration in the different environmental compartments.

7. Acknowledgement

This work was supported by the French National Program EC2CO (Ecosphère Continentale et Côtière), by the University of Savoie Mont-Blanc and by the IRS Program of the University of Grenoble Alpes. Chemical analysis at the Air-O-Sol facility at IGE was made possible with the funding of some of the equipment by the Labex OSUG@2020 (ANR10 LABX56). We acknowledge the work of C. Voiron (IGE) regarding chemical analysis of extracting solutions and the work of N. Findling (ISTerre) regarding XRD patterns acquisition and treatment. We also thank the three anonymous reviewers and the editor for valuable comments which significantly help to improve the original version of the manuscript.

8. Appendix A – Supplementary material

Supplementary material is available at the following link

9. References

Alloway, B. J. (Ed.). 2013. Heavy metals in soils: trace metals and metalloids in soils and their bioavailability.Volume. 22. Springer Science & Business Media. https://doi.org/10.1007/978-94-007-4470-7

Aplin, A.C., Matenaar, I.F., McCarty, D.K., van der Pluijm, B.A., 2006. Influence of mechanical compaction and clay mineral diagenesis on the microfabric and pore-scale properties of deep-water Gulf of Mexico mudstones. Clays and Clay Minerals 54, 500–514. https://doi.org/10.1346/CCMN.2006.0540411

Arnaud, F., Serralongue, J., Winiarski, T., Desmet, M., Paterne, M., 2006. Pollution au plomb dans la Savoie antique (II–IIIe s. apr. J.-C.) en relation avec une installation métallurgique de la cité de Vienne. Comptes Rendus Geoscience 338, 244–252. https://doi.org/10.1016/j.crte.2005.11.008

Bao, Z., Al, T., Couillard, M., Poirier, G., Bain, J., Shrimpton, H.K., Finfrock, Y.Z., Lanzirotti, A., Paktunc, D., Saurette, E., Hu, Y., Ptacek, C.J., Blowes, D.W., 2021. A cross scale investigation of galena oxidation and controls on mobilization of lead in mine waste rock. Journal of Hazardous Materials 412, 125-130. https://doi.org/10.1016/j.jhazmat.2021.125130

Barbier, V., 1875. La Savoie industrielle. Deuxième partie : Mines et métaux. Chaux, ciments, plâtres, poteries et tuileries. Horlogerie. Industries diverses. IIIème série des Mémoires de l'Académie de Savoie. Ed. A. Bottero. Available from : < https://gallica.bnf.fr/ark:/12148/bpt6k9660541k.texteImage>

Bertauts, M., Janots, E., Rossi, M., Duhamel-Achin., Boiron, M.-C., Airaghi, L., Lanari, P., Lach, P., Peiffert, C., Magnin, V. A new Alpine metallogenic model for the Pb-Ag deposits of Macôt-la Plagne and Peisey-Nancroix (Western Alps). Gesociences, in the special issue "The Making of the Alps". https://doi.org/10.3390/geosciences12090331

Brown, G.E., Foster, A.L., Ostergren, J.D., 1999. Mineral surfaces and bioavailability of heavy metals: A molecular-scale perspective. PNAS 96, 3388–3395. https://doi.org/10.1073/pnas.96.7.3388

Buatier, M.D., Sobanska, S., Elsass, F., 2001. TEM-EDX investigation on Zn- and Pb-contaminated soils. Applied Geochemistry 16, 1165–1177. https://doi.org/10.1016/S0883-2927(01)00015-4

Camizuli, E., Rossi, M., Gasquet, D., 2021. Trace metals dispersion from 1000 years of mining activity in the northern French Alps. The Extractive Industries and Society 8, 135–146. https://doi.org/10.1016/j.exis.2020.08.017

Camizuli, E., Scheifler, R., Garnier, S., Monna, F., Losno, R., Gourault, C., Hamm, G., Lachiche, C., Delivet, G., Chateau, C., Alibert, P., 2018. Trace metals from historical mining sites and past metallurgical activity remain bioavailable to wildlife today. Scientific Reports 8, 34-36. https://doi.org/10.1038/s41598-018-20983-0

CCME (Canadian Council of Ministres of the Environment), 2007. Canadian Soil Quality Guidelines for the Protection of Environmental and Human Health. Summary Tables, CCME Ottawa, Canada. Available from : https://ccme.ca/en/current-activities/canadian-environmental-quality-guidelines

Cappuyns, V., 2012. A Critical Evaluation of Single Extractions from the SMT Program to Determine Trace Element Mobility in Sediments. Applied and Environmental Soil Science 2012 in the special issue "Impact of Human Activities on Soil Contamination", Article ID 672914, 15 pages. https://doi.org/10.1155/2012/672914

Carignan, J., Hild, P., Mevelle, G., Morel, J., Yeghicheyan, D., 2001. Routine Analyses of Trace Elements in Geological Samples using Flow Injection and Low Pressure On-Line Liquid Chromatography Coupled to ICP-MS: A Study of Geochemical Reference Materials BR, DR-N, UB-N, AN-G and GH. Geostandards and Geoanalytical Research 25, 187–198. https://doi.org/10.1111/j.1751-908X.2001.tb00595.x

Causse, B., Spadini, L., Martins, J.M.F., Lenoir, T., Heyraud, A., Delolme, C., 2013. Xanthan exopolysaccharide: Acid–base reactivity related to structure and conformation. A model for understanding the reactivity of degraded and colloidal soil organic matter. Chemical Geology 359, 150–158. https://doi.org/10.1016/j.chemgeo.2013.09.010

Chester, R., Stoner, J.H., 1973. Pb in Particulates from the Lower Atmosphere of the Eastern Atlantic. Nature 245, 27–28. https://doi.org/10.1038/245027b0

Chopin, E.I.B., Alloway, B.J., 2007. Trace element partitioning and soil particle characterisation around mining and smelting areas at Tharsis, Ríotinto and Huelva, SW Spain. Science of The Total Environment 373, 488–500. https://doi.org/10.1016/j.scitotenv.2006.11.037

Cloquet, C., Carignan, J., Libourel, G., 2006. Atmospheric pollutant dispersion around an urban area using trace metal concentrations and Pb isotopic compositions in epiphytic lichens. Atmospheric Environment 40, 574–587. https://doi.org/10.1016/j.atmosenv.2005.09.073

Cortada, U., Hidalgo, M.C., Martínez, J., Rey, J., 2018. Impact in soils caused by metal(loid)s in lead metallurgy. The case of La Cruz Smelter (Southern Spain). Journal of Geochemical Exploration 190, 302–313. https://doi.org/10.1016/j.gexplo.2018.04.001

Cotter-Howells, J., 1996. Lead phosphate formation in soils. Environmental Pollution 93, 9–16. https://doi.org/10.1016/0269-7491(96)00020-6

Cotter-Howells, J., Thornton, I., 1991. Sources and pathways of environmental lead to children in a Derbyshire mining village. Environmental Geochemistry and Health 13, 127–135. https://doi.org/10.1007/BF01734304

Davis, A., Drexler, J.W., Ruby, M.V., Nicholson, A., 1993. Micromineralogy of mine wastes in relation to lead bioavailability, Butte, Montana. Environmental Science & Technology 27, 1415–1425. https://doi.org/10.1021/es00044a018

Doebelin, N., Kleeberg, R., 2015. Profex: a graphical user interface for the Rietveld refinement program BGMN. Journal of Applied Crystallography 48, 1573–1580. https://doi.org/10.1107/S1600576715014685

Doucet, F.J., Carignan, J., 2001. Atmospheric Pb isotopic composition and trace metal concentration as revealed by epiphytic lichens: an investigation related to two altitudinal sections in Eastern France. Atmospheric Environment 35, 3681–3690. https://doi.org/10.1016/S1352-2310(00)00510-0

EC (European Commission). 1986. Council Directive 86/278/EEC of 12 June 1986 on the protection of the environment, and in particular of the soil, when sewage sludge is used in agriculture. Available from : https://op.europa.eu/en/publication-detail/-/publication/f76faa39-2b27-42f2-be1e-9332f795e324/language-en

Elbaz-Poulichet, F., Guédron, S., Anne-Lise, D., Freydier, R., Perrot, V., Rossi, M., Piot, C., Delpoux, S., Sabatier, P., 2020. A 10,000-year record of trace metal and metalloid (Cu, Hg, Sb, Pb) deposition in a western Alpine lake (Lake Robert, France): Deciphering local and regional mining contamination. Quaternary Science Reviews 228, Article ID 106076. https://doi.org/10.1016/j.quascirev.2019.106076

Ettler, V., 2016. Soil contamination near non-ferrous metal smelters: A review. Applied Geochemistry64 in the special issue "Environmental Impacts of Mining and Smelting", 56–74. https://doi.org/10.1016/j.apgeochem.2015.09.020

Gałuszka, A., Migaszewski, Z.M., Dołęgowska, S., Michalik, A., Duczmal-Czernikiewicz, A., 2015. Geochemical background of potentially toxic trace elements in soils of the historic copper mining area: a case study from Miedzianka Mt., Holy Cross Mountains, south-central Poland. Environmental Earth Sciences 74, 4589–4605. https://doi.org/10.1007/s12665-015-4395-6

Garçon, A.-F., Ph.D. thesis, 1995. Les métaux non ferreux en France aux XVIIIe et XIXe siècles : Ruptures, blocages, évolution au sein des systèmes techniques. Paris, EHESS. Available from : < http://www.theses.fr/1995EHES0061>

Guillevic, F., Rossi, M., Poulenard, J., Sabatier, P., Develle, A-L., Quantin, C., Monvoisin, G., Arnaud, F., The delayed response of an atmospheric contamination in mountainous catchment. In prep**.** for Science of the Total Environment (STOTEN).

Hansson, S.V., Claustres, A., Probst, A., De Vleeschouwer, F., Baron, S., Galop, D., Mazier, F., Le Roux, G., 2017. Atmospheric and terrigenous metal accumulation over 3000 years in a French mountain catchment: Local vs distal influences. Anthropocene 19, 45–54. https://doi.org/10.1016/j.ancene.2017.09.002

Heiri, O., Lotter, A.F., Lemcke, G., 2001. Loss on ignition as a method for estimating organic and carbonate content in sediments: reproducibility and comparability of results. Journal of Paleolimnology 25, 101–110. https://doi.org/10.1023/A:1008119611481

Hettiarachchi, G.M., Pierzynski, G.M., Ransom, M.D., 2000. In Situ Stabilization of Soil Lead Using Phosphorus and Manganese Oxide. Environmental Science & Technology. 34, 4614–4619. https://doi.org/10.1021/es001228p

Hong, S., Candelone, J.-P., Patterson, C.C., Boutron, C.F., 1994. Greenland Ice Evidence of Hemispheric Lead Pollution Two Millennia Ago by Greek and Roman Civilizations. Science 265, 1841–1843. https://doi.org/10.1126/science.265.5180.1841

Judet, P., 2014. Exploitation, abandon et patrimonialisation des mines savoyardes de 1750 à nos jours. Une introduction à une histoire longue et contrastée. Collection EDYTEM. Cahiers de géographie 17, 53–60. https://doi.org/10.3406/edyte.2014.1273

Keim, M.F., Markl, G., 2015. Weathering of galena: Mineralogical processes, hydrogeochemical fluid path modeling, and estimation of the growth rate of pyromorphite. American Mineralogist 100, 1584–1594. https://doi.org/10.2138/am-2015-5183

Kříbek, B., Nyambe, I., Majer, V., Knésl, I., Mihaljevič, M., Ettler, V., Vaněk, A., Penížek, V., Sracek, O., 2019. Soil contamination near the Kabwe Pb-Zn smelter in Zambia: Environmental impacts and remediation measures proposal. Journal of Geochemical Exploration 197, 159–173. https://doi.org/10.1016/j.gexplo.2018.11.018

Lejon, D.P.H., Martins, J.M.F., Lévêque, J., Spadini, L., Pascault, N., Landry, D., Milloux, M.-J., Nowak, V., Chaussod, R., Ranjard, L., 2008. Copper Dynamics and Impact on Microbial Communities in Soils of Variable Organic Status. Environmental Science &Technology 42, 2819–2825. https://doi.org/10.1021/es071652r

Mariet, A.-L., Sarret, G., Bégeot, C., Walter-Simonnet, A.-V., Gimbert, F., 2017. Lead Highly Available in Soils Centuries after Metallurgical Activities. Journal of Environmental Quality 46, 1236–1242. https://doi.org/10.2134/jeq2016.12.0469

Meloux, J., 1975. Alpes-Nord : Bilan synthétique de dix années de prospection. Rapport BRGM n°75- RME- 023-FE. BRGM, Orléans, France, 104p.

Monna, F., Camizuli, E., Revelli, P., Biville, C., Thomas, C., Losno, R., Scheifler, R., Bruguier, O., Baron, S., Chateau, C., Ploquin, A., Alibert, P., 2011. Wild Brown Trout Affected by Historical Mining in the Cévennes National Park, France. Environmental Science & Technology. 45, 6823–6830. https://doi.org/10.1021/es200755n

Morin, G., Juillot, F., Ildefonse, P., Calas, G., Samama, J.-C., Chevallier, P., Brown, G.E., 2001. Mineralogy of lead in a soil developed on a Pb-mineralized sandstone (Largentière, France). American Mineralogist 86, 92–104. https://doi.org/10.2138/am-2001-0110

Müller, G., 1979. Schwermetalle in den sediments des Rheins-Veranderungen seit 1971.Umschau in Wissenschaft und Technik79, 778–783.

Navel, A., Martins, J.M.F., 2014. Effect of long-term organic amendments and vegetation of vineyard soils on the microscale distribution and biogeochemistry of copper. Science of The Total Environment 466–467, 681–689. https://doi.org/10.1016/j.scitotenv.2013.07.064

Navel, A., Uzu, G., Spadini, L., Sobanska, S., Martins, J.M.F., 2015. Combining microscopy with spectroscopic and chemical methods for tracing the origin of atmospheric fallouts from mining sites. Journal of Hazardous Materials 300, 538–545. https://doi.org/10.1016/j.jhazmat.2015.07.035

Nriagu, J.O., 1974. Lead orthophosphates—IV Formation and stability in the environment. Geochimica et Cosmochimica Acta 38, 887–898. https://doi.org/10.1016/0016-7037(74)90062-3

Ostergren, J.D., Brown, Gordon E., Parks, G.A., Tingle, T.N., 1999. Quantitative Speciation of Lead in Selected Mine Tailings from Leadville, CO. Environmental Science & Technology 33, 1627–1636. https://doi.org/10.1021/es980660s

Peloux, F., Bailly-Maître, M.-C., Viallet, H., 2015. L'histoire si curieuse des mines de Brandes. Grenoble : Presses universitaires de Grenoble.

Quevauviller, P., 1998. Operationally defined extraction procedures for soil and sediment analysis I. Standardization. Trends in Analytical Chemistry 17, 289–298. https://doi.org/10.1016/S0165-9936(97)00119-2

Rao, C.R.M., Sahuquillo, A., Lopez Sanchez, J.F., 2008. A review of the different methods applied in environmental geochemistry for Single and sequential extraction of trace elements in soils and related materials. Water Air Soil Pollution 189, 291–333. https://doi.org/10.1007/s11270-007-9564-0

Reimann, C., de Caritat, P., 2000. Intrinsic flaws of element enrichment factors (EFs) in environmental geochemistry. Environmental Science & Technology 34, 5084–5091. https://doi.org/10.1021/es001339o

Rudnick, R.L., Gao, S., 2003. Composition of the continental crust. In: Holland, H.D., Turekian, K.K. (Eds.), Treatise on Geochemistry, Vol. 3. Elsevier, Amsterdam, Netherlands, pp. 1–64

Sahuquillo, A., Rigol, A., Rauret, G., 2003. Overview of the use of leaching/extraction tests for risk assessment of trace metals in contaminated soils and sediments. TrAC Trends in Analytical Chemistry 22, 152–159. https://doi.org/10.1016/S0165-9936(03)00303-0

Spadini, L., Navel, A., Martins, J.M.F., Vince, E., Lamy, I., 2018. Soil aggregates: a scale to investigate the densities of metal and proton reactive sites of organic matter and clay phases in soil. European Journal of Soil Science 69, 953–961. https://doi.org/10.1111/ejss.12695

Sterckeman, T., Gomez, A., Ciesielski, H., 1996. Soil and waste analysis for environmental risk assessment in France. Science of The Total Environment 178 in the special issue "Harmonization of Leaching/Extraction Tests for Environmental Risk Assessment", 63–69. https://doi.org/10.1016/0048-9697(95)04798-0

Stoffers, P., Glasby, G.P., Wilson, C.J., Davis, K.R., Walter, P., 1986. Heavy metal pollution in Wellington Harbour. New Zealand Journal of Marine and Freshwater Research 20, 495–512. https://doi.org/10.1080/00288330.1986.9516169

Swęd, M., Uzarowicz, Ł., Duczmal-Czernikiewicz, A., Kwasowski, W., Pędziwiatr, A., Siepak, M., Niedzielski, P., 2022. Forms of metal(loid)s in soils derived from historical calamine mining waste and tailings of the Olkusz Zn–Pb ore district, southern Poland: A combined pedological, geochemical and mineralogical approach. Applied Geochemistry 139, Article ID 105218. https://doi.org/10.1016/j.apgeochem.2022.105218

Thiombane, M., Di Bonito, M., Albanese, S., Zuzolo, D., Lima, A., De Vivo, B., 2019. Geogenic versus anthropogenic behaviour and geochemical footprint of Al, Na, K and P in the Campania region (Southern Italy) soils through compositional data analysis and enrichment factor. Geoderma 335, 12–26. https://doi.org/10.1016/j.geoderma.2018.08.008

van der Voet, E., Salminen, R., Eckelman, M., Norgate, T., Mudd, G., Hisschier, R., Spijker, J., Vijver, M., Selinus, O., Posthuma, L., de Zwart, D., van de Meent, D., Reuter, M., Tikana, L., Valdivia, S., Wäger, P., Hauschild, M.Z., de Koning, A., 2013. Environmental challenges of anthropogenic metals flows and cycles (Report No. 978-92-807-3266–5), Environmental challenges of anthropogenic metals flows and cycles. United Nations Environment Programme. Available from : https://www.unep.org/resources/report/environmental-risks-and-challenges-anthropogenic-metals-flows-and-cycles

Vuong, X.T., Prietzel, J., Heitkamp, F., 2016. Measurement of organic and inorganic carbon in dolomite-containing samples. Soil Use and Management 32, 53–59. https://doi.org/10.1111/sum.12233

Zdanowicz, C.M., Banic, C.M., Paktunc, D.A., Kliza-Petelle, D.A., 2006. Metal emissions from a Cu smelter, Rouyn-Noranda, Québec: characterization of particles sampled in air and snow. Geochemistry: Exploration, Environment, Analysis 6, 147–162. https://doi.org/10.1144/1467-7873/05-089

10. Figure captions

Figure 1: A) Location map of Peisey-Nancroix in the northern French Alps; B) Geological map of the Peisey-Nancroix Pb-Ag mine and its surroundings; C) Organisation of the old mine site, and infrastructures still present today divided between the ore-processing site (O.P.) to the north and the ore-smelting (O.S.) site to the southeast, where waste rock heaps and slag heaps are located.

Figure 2: Reflected light (A) and SEM images (B-K) of primary and secondary Pb-bearing phases identified in the ore (A), slags (B-C) and soils (D-K). In Pb-bearing primary contamination phases: A) galena (Gn.)-, pyrite (Py.), and tetrahedrite (Ttr.) from the ore; B) rounded-shaped PbO with empty holes in the centre observed in slags; C) Fe-sulfides mixed with PbO phases in slags. In weathered Pb-bearing primary contamination phases in soils: D) galena particles altered into cerussite (cerussite I); E) weathered slag particles with micrometric to tens of micrometres-sized Pb prills in a Pb-enriched silicate matrix. In secondary reprecipitated Pb-bearing phases in soils: F) cerussite particles with relict galena (cerussite I); G) reprecipitated cerussite (cerussite II); H) rounded nanometric aggregate of Pb-bearing Mn (hydr-)oxides; I) aggregate of Pb-bearing Mn (hydr-)oxides; J) pyromorphite; K) rounded aggregates of pyromorphite.

Figure 3: A) Principal component analysis of the 117 samples based on major elements and soil organic matter (SOM) with Pb as an illustrative supplementary variable, allowing the characterisation of three soil types: carbonate-rich cambisols, carbonate-poor cambisols and highly contaminated soils; B) Distribution map of the three soil types.

Figure 4: A) Spatial distribution of the total Pb content in soils indicating that Pb content decreases down to the local pedo-geochemical background (blue points); B) the Pb enrichment factor and; C) the Pb geoaccumulation index. Represented in A: waste rock heap (light grey), slag heap (dark grey), former mine and metallurgical buildings (black), underground dewatering gallery (wide dotted line) and footpath (small dotted line).

Figure 5: Spatial distribution of the Pb-bearing phases based on mineralogical observations: A- primary contamination phases (slags and ore particles) observed in soils based on binocular (> 2 mm, n = 117)) and SEM (< 2 mm, n = 19) observations. B- the Pb-bearing secondary phases observed in soils, based on SEM (< 2 mm) observations only (n = 19).

Figure 6: Graph of the amount of extracted Pb ($mg.kg^{-1}$) using 3 extractants (distilled water, humic acid, and EDTA) as a function of the total soil Pb content ($mg.kg^{-1}$) on a logarithmic scale.

Figure 7: Spatial distribution of the fraction of extracted Pb (%) for each extractant: distilled water (in black circles), humic acid (in white circles) and EDTA (in grey circles). The 3 extraction groups were distinguished according to the amount of extracted Pb with distilled water and EDTA, the Pb contamination (EF_{Pb}) and the proximity of the slag heap (see text).

11. Tables

Table 1 : Major and trace element contents of waste rocks and slags

	Unit	Waste Rock 1	Waste Rock 2	Waste Rock 3	Slag 1	Slag 2	Slag 3
SiO_2		81.10	84.13	83.02	38.72	42.55	40.46
Al_2O_3		5.74	0.54	5.86	5.34	6.19	6.22
Fe_2O_3		1.11	1.10	1.04	18.90	20.60	21.13
MnO		0.08	0.07	0.08	1.15	1.29	0.60
MgO		0.97	0.55	0.98	2.22	2.37	2.57
CaO	*wt. %*	1.42	1.53	1.39	8.43	8.93	8.63
Na_2O		0.08	0.06	0.08	0.84	1.01	0.92
K_2O		1.94	0.17	1.97	1.71	1.89	1.91
TiO_2		0.06	< L.D.	0.06	0.31	0.35	0.45
P_2O_5		< L.D.	0.20	< L.D.	0.39	0.40	0.53
CO_2		3.73	3.77	2.53	-0.64	-0.67	-1.17
As		31	18	37	31	22	22
Cd		3	3	6	0.2	0.1	0.9
Cu		71	2018	87	239	335	143
Ni	$mg.kg^{-1}$	12	46	5	21	24	< L.D.
Pb		**29846**	**71384**	**18621**	**108418**	**75516**	**22694**
Sb		**128**	**112**	**137**	**1638**	**931**	**452**
Zn		**125**	**111**	**114**	**3790**	**3730**	**5276**

Waste rock 1 : PN17-R-07; Waste rock 2 : PN21-R-05; and Waste rock 3 : PN17-R-07

Slag 1 :PN21-SCO-01; Slag 2: PN21-SCO-03; and Slag 3 : PN17-R-14

Table 2 : Basic statistics of the 3 groups of soil based on PCA and hierarchical clustering (highly Pb-contaminated soil: highly Pb-cont.; carbonate-rich soil: carb. rich; and carbonate-poor soil: carb. poor).

Component	Unit	Min.				Q10				Q25				Q50 (mediane)				Q75				Q90				Maximum				IQR				Skewness				Kurtosis			
		All data	Highly Pb- cont.[1]	Carb. rich[1]	Carb. poor[1]	All data	Highly Pb- cont.	Carb. rich	Carb. poor	All data	Highly Pb- cont.	Carb. rich	Carb. poor	All data	Highly Pb- cont.	Carb. rich	Carb. poor	All data	Highly Pb- cont.	Carb. rich	Carb. poor	All data	Highly Pb- cont.	Carb. rich	Carb. poor	All data	Highly Pb- cont.	Carb. rich	Carb. poor	All data	Highly Pb- cont.	Carb. rich	Carb. poor	All data	Highly Pb- cont.	Carb. rich	Carb. poor	All data	Highly Pb- cont.	Carb. rich	Carb. poor
Na_2O		0.50	0.56	0.50	0.99	0.64	0.65	0.54	1.44	0.95	0.71	0.59	1.56	1.51	0.99	0.67	1.71	1.75	1.32	0.86	1.95	2.10	1.38	0.94	2.32	2.57	1.49	1.08	2.57	0.80	0.61	0.27	0.39	-0.02	-0.01	0.50	0.53	-0.88	-1.62	-1.12	-0.16
MgO		1.17	1.17	5.86	1.29	1.84	1.58	7.26	2.17	2.93	1.96	7.68	3.03	3.58	2.55	9.04	3.50	4.22	3.56	10.15	3.70	8.75	4.53	10.75	4.02	12.52	5.56	12.52	4.97	1.29	1.60	2.47	0.66	1.56	0.74	0.07	-0.76	1.65	-0.33	-0.79	0.76
Al_2O_3		3.64	3.64	4.22	12.08	7.60	7.10	4.92	13.88	11.14	8.19	6.23	14.73	14.46	12.15	8.00	15.53	15.63	13.47	9.76	15.98	16.29	14.40	10.32	16.52	19.00	15.55	11.75	19.00	4.49	5.28	3.53	1.25	-0.99	-0.51	-0.05	-0.39	-0.15	-0.87	-1.36	1.09
SiO_2		###	24.43	16.89	41.77	28.15	28.95	19.05	48.65	36.91	32.05	21.14	51.14	50.24	43.19	26.59	52.91	53.48	46.72	31.34	55.72	56.87	47.75	32.63	57.85	70.40	52.43	36.08	70.40	16.57	14.67	10.20	4.58	-0.71	-0.36	-0.03	0.86	-0.40	-1.38	-1.39	2.18
P_2O_5		0.06	0.12	0.06	0.10	0.13	0.15	0.13	0.12	0.15	0.16	0.16	0.14	0.19	0.22	0.21	0.18	0.24	0.28	0.27	0.22	0.28	0.35	0.31	0.24	0.56	0.56	0.36	0.29	0.09	0.12	0.10	0.07	1.52	1.41	-0.08	0.21	4.74	1.92	-0.87	-0.95
K_2O	(wt. %)	0.72	0.72	0.90	2.27	1.44	1.16	1.00	2.44	2.07	1.69	1.26	2.55	2.53	2.09	1.56	2.83	2.98	2.49	1.91	3.09	3.18	3.01	2.05	3.22	4.44	3.67	2.26	4.44	0.91	0.79	0.65	0.54	-0.25	0.06	-0.03	1.41	0.13	-0.36	-1.38	2.69
CaO		0.33	0.80	10.90	0.33	0.83	1.33	12.10	0.79	1.29	2.06	12.94	0.89	2.42	3.24	17.26	1.68	7.29	5.76	19.46	2.48	15.73	10.12	23.34	4.49	25.75	15.40	25.75	11.56	6.00	3.70	6.52	1.59	1.52	1.41	0.41	2.30	1.27	1.14	-0.95	5.11
TiO_2		0.17	0.23	0.17	0.41	0.35	0.28	0.26	0.62	0.50	0.39	0.31	0.70	0.68	0.56	0.39	0.76	0.78	0.62	0.50	0.80	0.81	0.70	0.51	0.86	0.99	0.75	0.61	0.99	0.28	0.23	0.18	0.10	-0.58	-0.32	-0.08	-0.61	-0.58	-1.22	-1.02	1.17
MnO		0.02	0.07	0.02	0.06	0.06	0.08	0.03	0.07	0.08	0.11	0.03	0.09	0.10	0.12	0.05	0.10	0.11	0.16	0.07	0.11	0.14	0.21	0.09	0.12	0.37	0.37	0.09	0.17	0.03	0.06	0.04	0.02	2.40	1.71	0.19	0.39	10.87	2.98	-1.42	1.52
Fe_2O_3		2.29	3.29	2.29	3.22	4.29	3.93	4.20	4.94	5.54	4.63	4.69	6.19	6.25	5.55	5.87	6.40	6.78	6.22	6.88	6.82	7.32	7.08	7.13	7.30	8.15	7.95	7.67	8.15	1.24	1.59	2.18	0.63	-0.76	0.17	-0.50	-1.18	0.26	-0.74	-0.47	1.81
S.O.M. (LOI, %)		1.10	9.50	4.20	1.10	5	14.06	12.15	4.08	7.9	15.2	13.7	6.42	11.00	18.60	16.70	9.20	15.5	28.3	24.9	10.67	26.88	41.04	29.6	13.42	55.3	49.5	55.3	19.1	7.6	13.1	11.20	4.25	1.88	1.02	1.49	0.26	3.92	-0.31	2.29	0.09
Carb.		0.50	0.50	5.40	1.30	1.70	1.66	15.05	1.60	1.90	2.30	16.82	1.80	2.60	3.20	22.30	2.20	7.10	6.85	24.18	3.08	20.30	12.30	26.22	4.27	31.50	12.70	31.50	10.90	5.20	4.55	7.35	1.28	1.69	1.02	-0.64	2.46	1.62	-0.46	0.28	5.77
Cu		9	26	9	17	22	42	12	23	27	46	19	27	36	83	25	35	47	99	31	40	84	131	45	50	551	551	55	64	20	53	12	13	7.14	3.73	0.54	0.65	62.23	14.67	-0.49	0.20
Zn		35	91	35	71	82	102	56	90	98	178	68	99	116	256	95	114	160	307	127	125	262	411	163	148	1202	1202	184	236	63	130	59	26	5.37	2.95	0.45	1.56	38.85	10.12	-1.03	4.29
Pb	(mg.kg-1)	5	1560	141	5	41	3070	488	17	355	5942	752	130	1173	12249	1272	467	4236	18211	3463	1428	13157	34915	6041	2114	37609	37609	6449	5781	3882	12269	2710	1298	2.78	0.88	0.94	2.08	7.79	-0.41	-0.79	3.92
Sb		2	4	2	0	2	16	2	2	3	27	2	3	6	67	2	5	20	128	7	10	75	155	16	23	407	407	17	52	17	102	7	6	4.08	1.97	1.05	2.24	22.29	5.11	-0.68	4.85

[1] highly contaminated soil (n=27); carbonate-rich soil (n=20); and carbonate-poor soil (n=70)

Table 3 : PTE content of site reference soils and rocks and guidelines.

PTE	Site reference (in mg.kg^{-1})				Guidelines (in mg.kg^{-1})	
	Distant topsoil[1]	Deep-horizon soil[1]	Average watershed rocks[2]	Continental crust[3]	CCME[4]	E.U.[5]
Pb	87	123	17	17	70/140	300
Sb	2	5	2	0.4	20	-
Cu	15	34	17	28	63	140
Zn	126	77	94	67	250	300

[1] n = 2; one soil sampled 2 km upstream of the mining site and one deep horizon soil from the mining site

[2] n = 34 rocks
[3] Rudnick & Gao 2003
[4] CCME (Canadian Council of Ministres of the Environment) 2007
[5] EC Directive 86/278/EEC (Agricultural and after sewage sludge application)

Table 4: Spearman correlations between the Pb total content and major elements and constituents of soil.

		MnO		P_2O_5		Sb		$Carbonates_{950°}$		$SOM_{550°}$	
	Group of soil type	All samples	Per soil type	All samples	Per soil type	All samples	Per soil type	All samples	Per soil type	All samples	Per soil type
Pb	CPS		**0.37**		0.27		**0.93**		-0.03		**0.33**
	CRS	**0.58**	**0.82**	**0.57**	**0.67**	**0.79**	**0.91**	-0.08	**-0.7**	**0.43**	0.22
	HCS		0.44		**0.68**		0.61		-0.13		-0.07

Statistically significant correlation at probability levels: $p<0.05$, **$p<0.01$**, and **$p<0.001$**

Table 5 : Classification of samples in groups of Pb extraction variability.

	Slope	Distance from sources	Pb contamination	Pb mobility		Potential mobilisation	Samples
			EF_{Pb}	Distilled water	Humic acid	EDTA	
Group 1	Off slope	Distal	EF <4	Non quantifiable	Non quantifiable to low (> 0.20 %)	Low (< 60 %)	G8, H11, K1 (EF_{Pb} = 5), K9
Group 2	Downslope	Distal	4 < EF < 40	Non quantifiable to low (< 0.10 %)	Low (< 0.20 %)	Median (60 to 80 %)	B4 (EF_{Pb} = 2), K4, K5, M3, M5, P2
Group 3	Downslope	Proximal	EF > 40	High (> 0.10 %)	High (> 0.20 %)	High (> 80 %)	AA1, B2A, D3, E3, G3, G5, H5, I3, L2, N4 (EF_{Pb} = 10), O1

Table 6 : Spearman correlation coefficients between extracted Pb and soil properties (n = 20).

	pH	TOC	CEC	$CaCO_{3T}$	Mn_{ex}	Ca_{ex}	Pb_{total}
Pb_{total}	0.12	**0.79**	**0.7**	0.49	0.12	0.62	1
$Pb_{distill.water}$	-0.08	0.63	0.55	0.33	0.25	0.43	**0.93**
$Pb_{hum.acid}$	-0.10	0.61	0.50	0.26	0.20	0.38	**0.92**
Pb_{EDTA}	0.08	**0.74**	0.64	0.45	0.11	0.53	**0.98**

ex. exchangeable cation
Statistically significant correlation at probability levels: $p<0.05$, **$p<0.01$**, and **$p<0.001$**

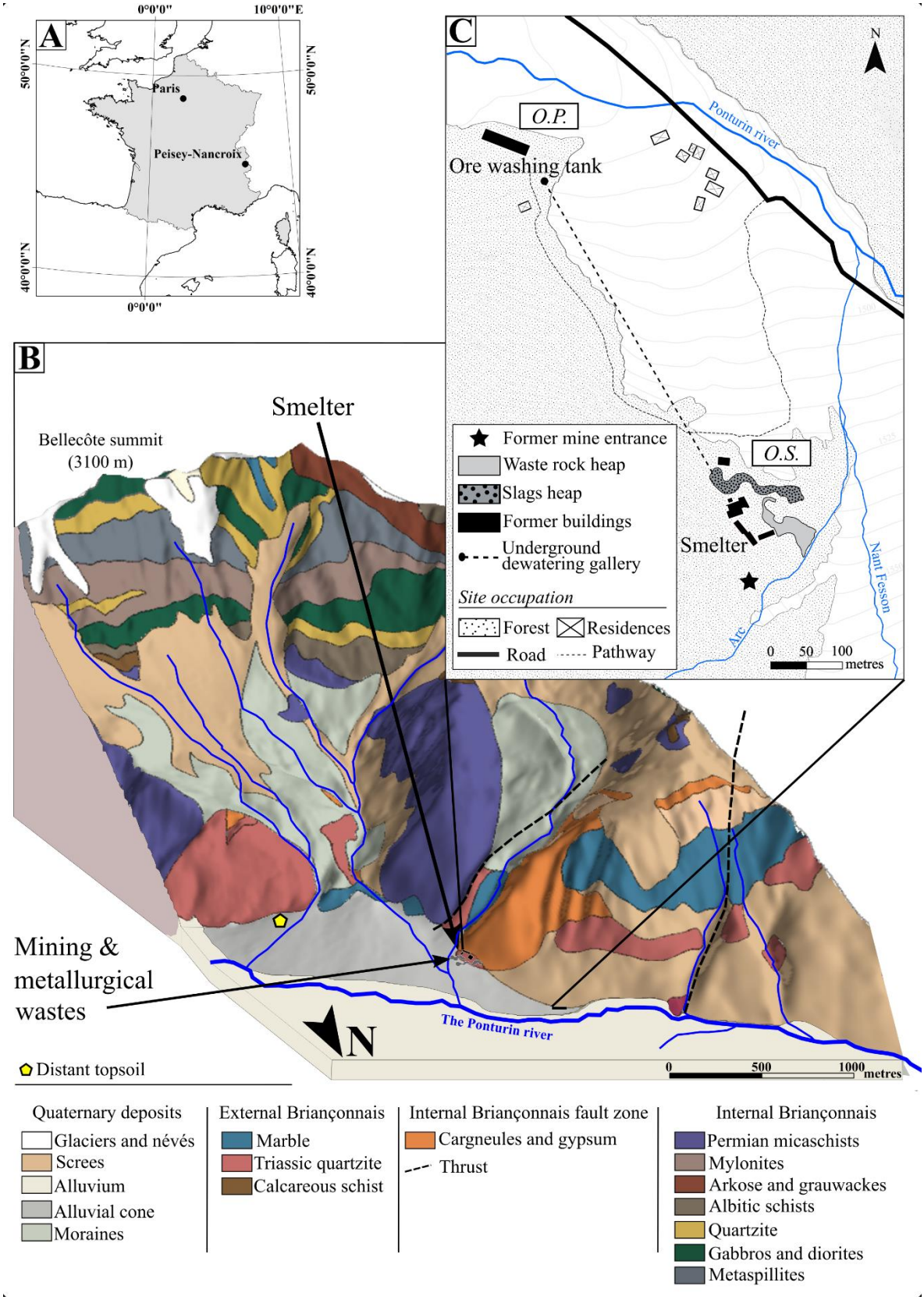

Figure 1: A) Location map of Peisey-Nancroix in the northern French Alps; B) Geological map of the Peisey-Nancroix Pb-Ag mine and its surroundings; C) Organisation of the old mine site, and infrastructures still present today divided between the ore-processing site (O.P.) to the north and the ore-smelting (O.S.) site to the southeast, where waste rock heaps and slag heaps are located.

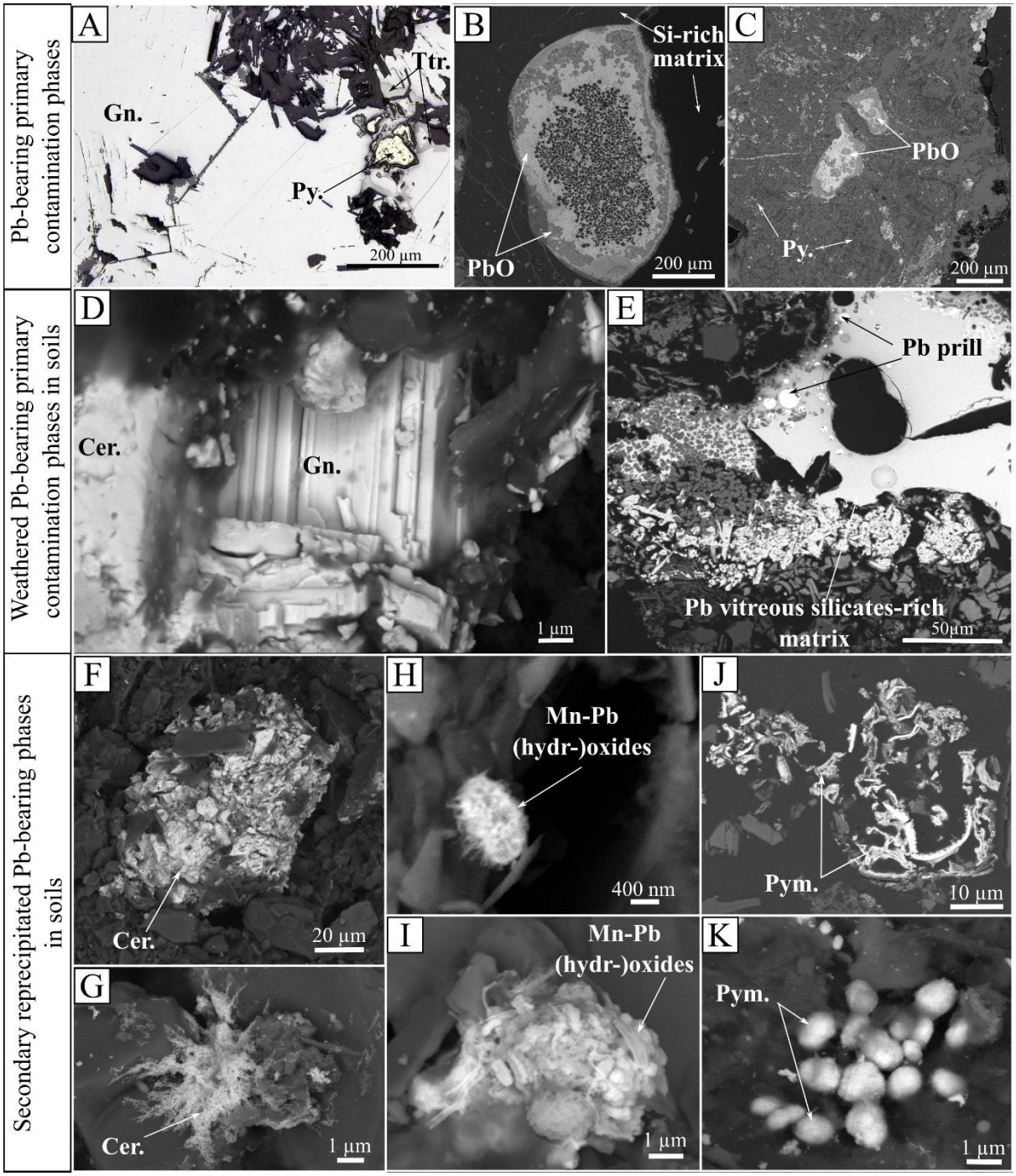

Figure 2: Reflected light (A) and SEM images (B-K) of primary and secondary Pb-bearing phases identified in the ore (A), slags (B-C) and soils (D-K). In Pb-bearing primary contamination phases: A) galena (Gn.)-, pyrite (Py.), and tetrahedrite (Ttr.) from the ore; B) rounded-shaped PbO with empty holes in the centre observed in slags; C) Fe-sulfides mixed with PbO phases in slags. In weathered Pb-bearing primary contamination phases in soils: D) galena particles altered into cerussite (cerussite I); E) weathered slag particles with micrometric to tens of micrometres-sized Pb prills in a Pb-enriched silicate matrix. In secondary reprecipitated Pb-bearing phases in soils: F) cerussite particles with relict galena (cerussite I); G) reprecipitated cerussite (cerussite II); H) rounded nanometric aggregate of Pb-bearing Mn (hydr-)oxides; I) aggregate of Pb-bearing Mn (hydr-)oxides; J) pyromorphite; K) rounded aggregates of pyromorphite.

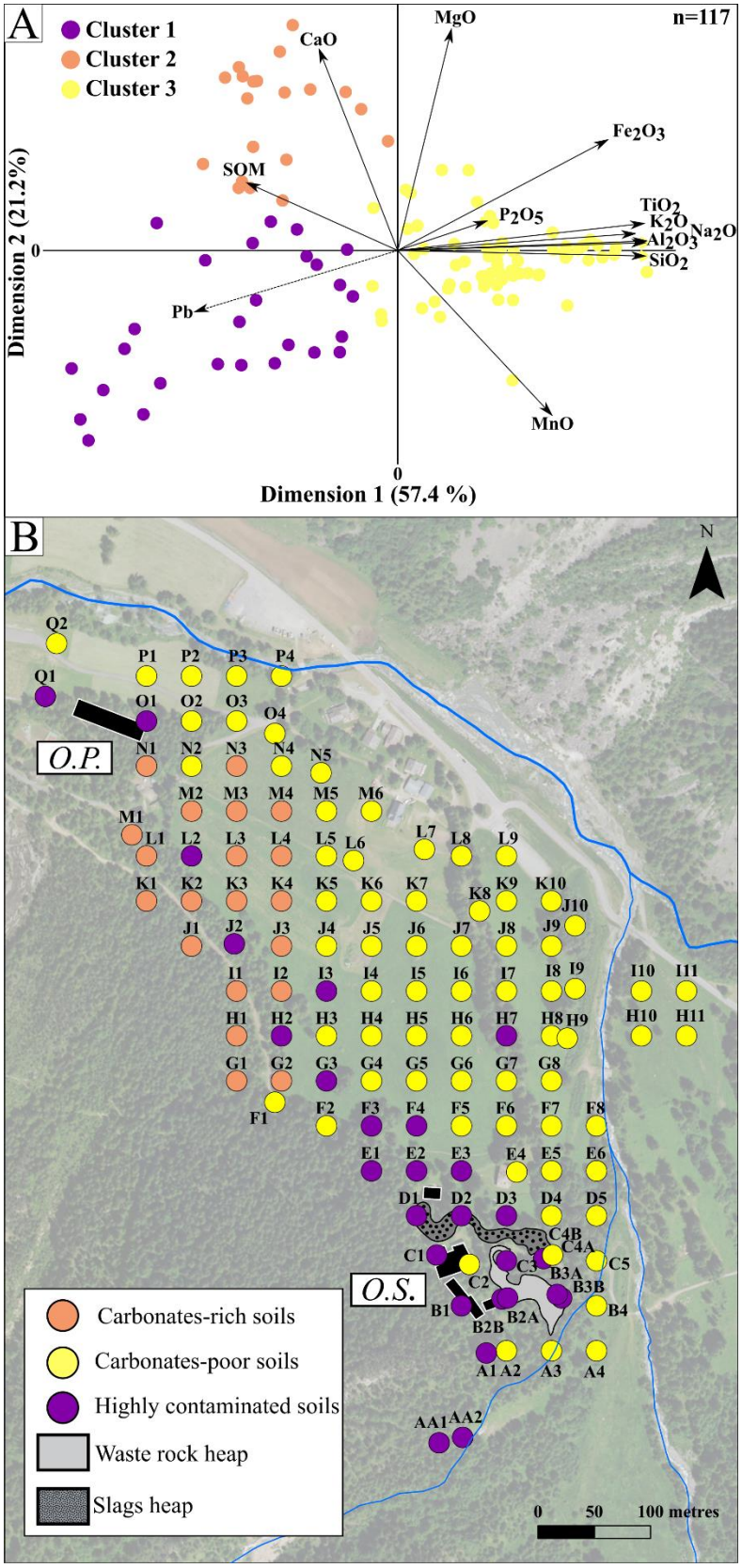

Figure 3: A) Principal component analysis of the 117 samples based on major elements and soil organic matter (SOM) with Pb as an illustrative supplementary variable, allowing the characterisation of three soil types: carbonate-rich cambisols, carbonate-poor cambisols and highly contaminated soils; B) Distribution map of the three soil types.

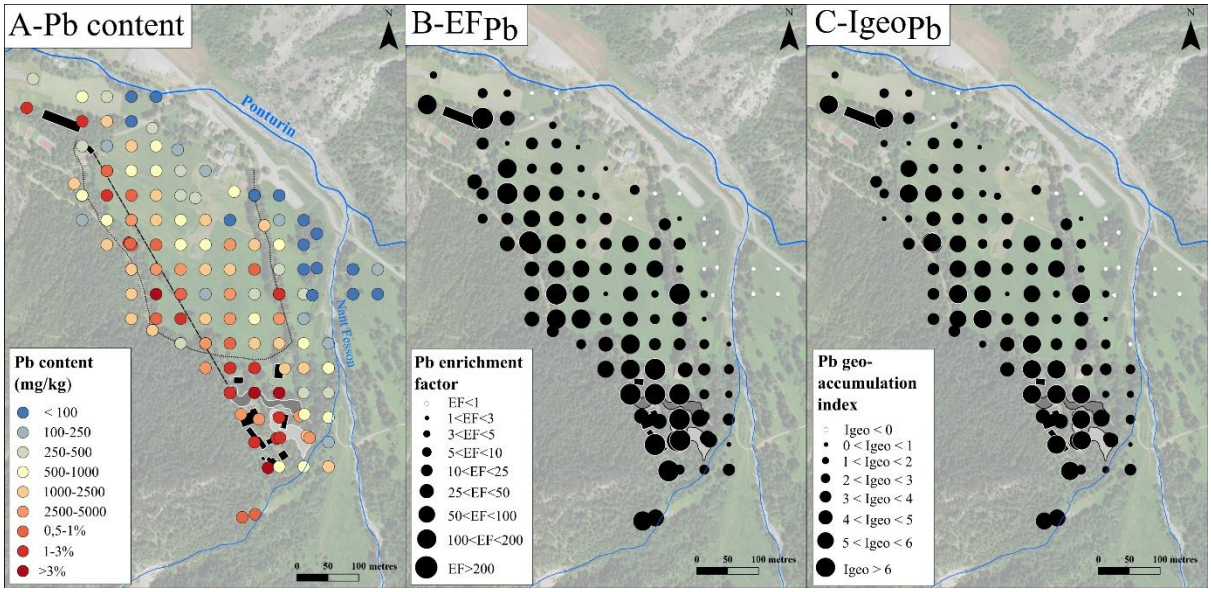

Figure 4: A) Spatial distribution of the total Pb content in soils indicating that Pb content decreases down to the local pedo-geochemical background (blue points); B) the Pb enrichment factor and; C) the Pb geoaccumulation index. Represented in A: waste rock heap (light grey), slag heap (dark grey), former mine and metallurgical buildings (black), underground dewatering gallery (wide dotted line) and footpath (small dotted line).

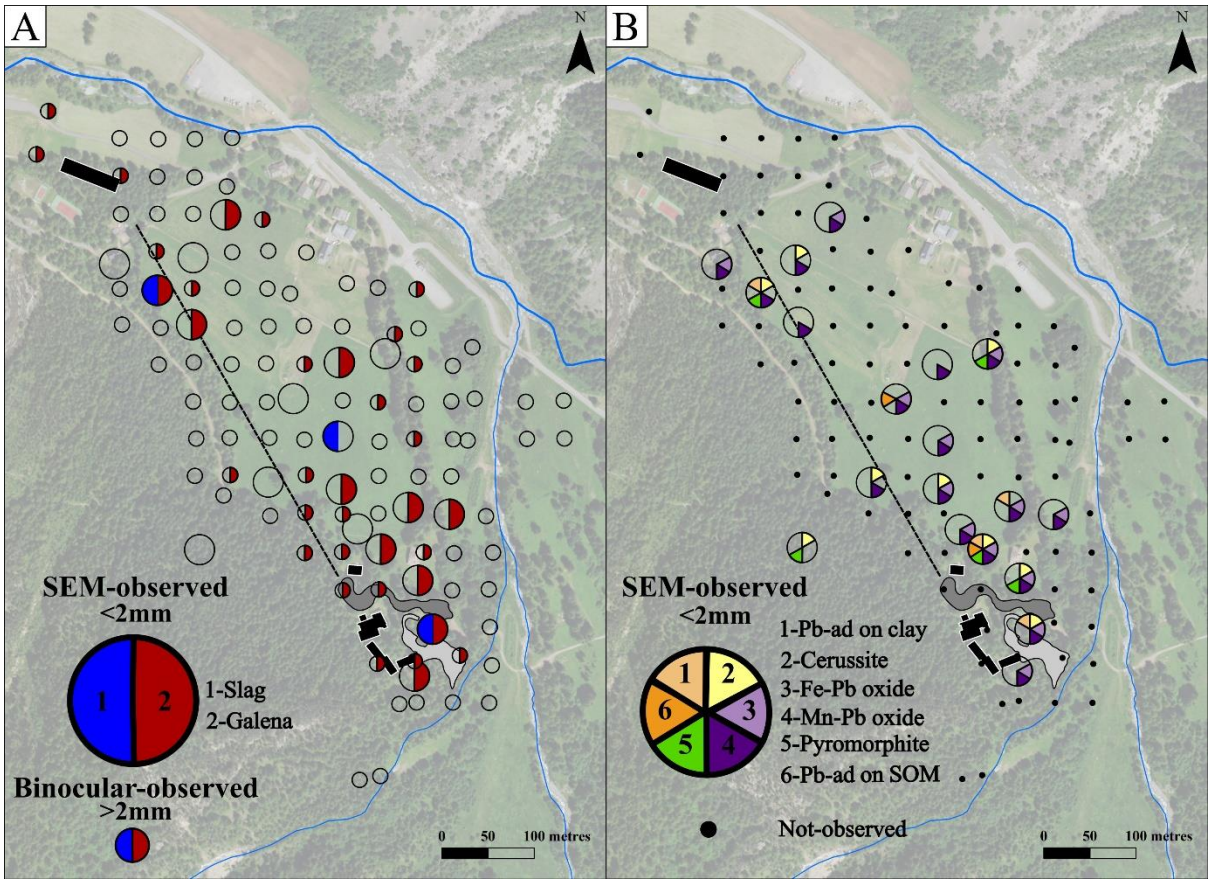

Figure 5: Spatial distribution of the Pb-bearing phases based on mineralogical observations: A-primary contamination phases (slags and ore particles) observed in soils based on binocular (> 2 mm, n = 117)) and SEM (< 2 mm, n = 19) observations. B- the Pb-bearing secondary phases observed in soils, based on SEM (< 2 mm) observations only (n = 19).

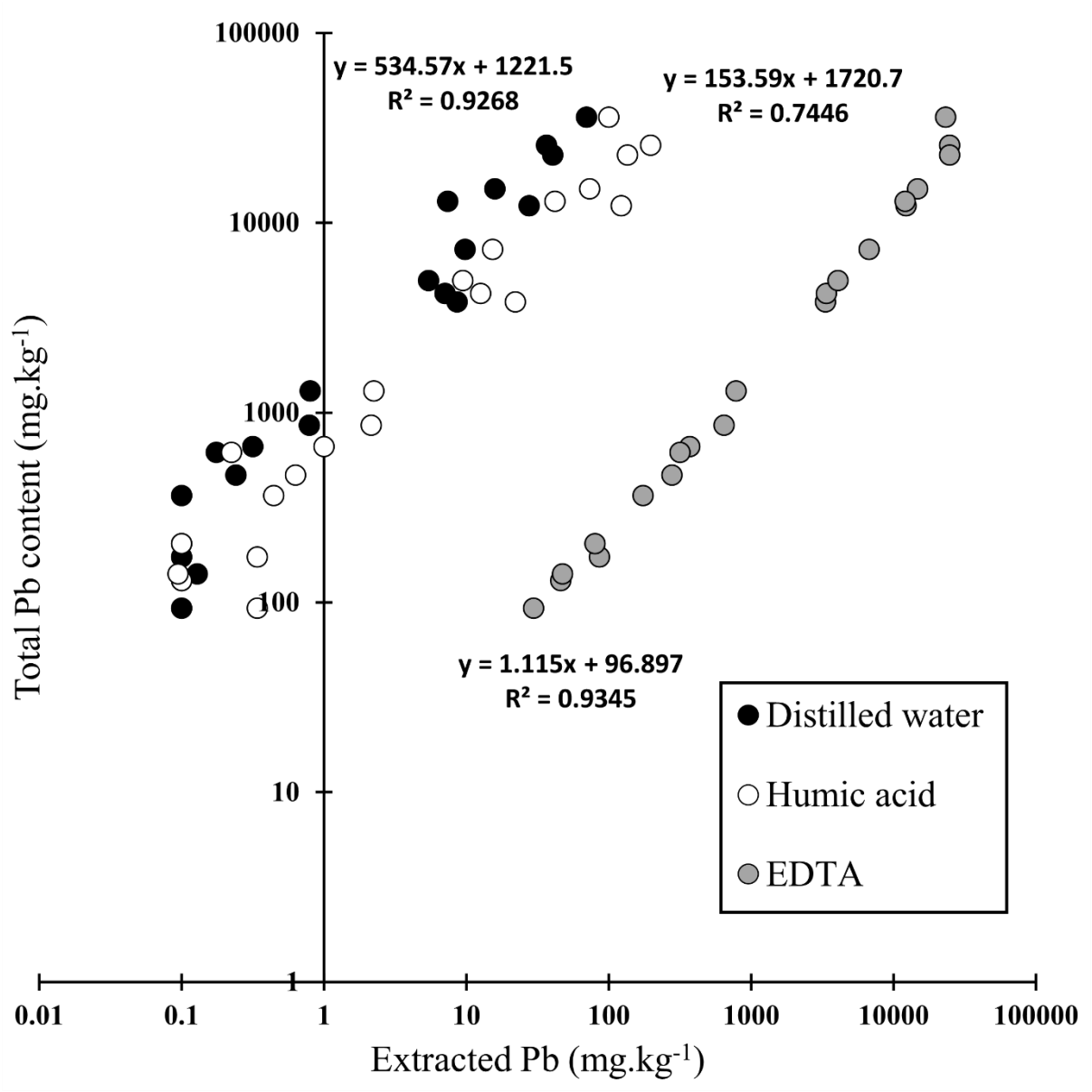

Figure 6: Graph of the amount of extracted Pb ($mg.kg^{-1}$) using 3 extractants (distilled water, humic acid, and EDTA) as a function of the total soil Pb content ($mg.kg^{-1}$) on a logarithmic scale.

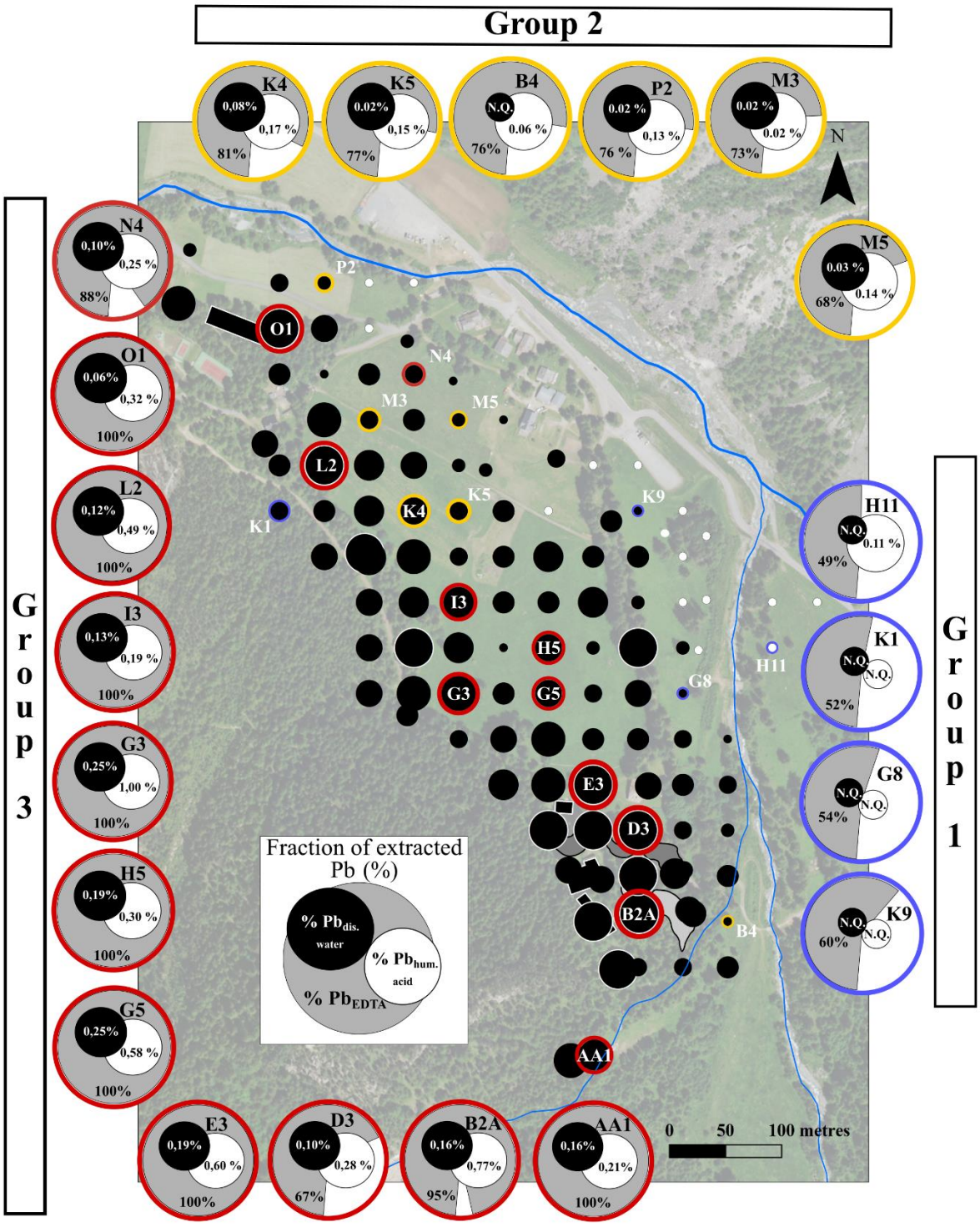

N.Q. (Non Quantifiable) Measured Pb content from the initial solution is under the limit of quantification.

Figure 7: Spatial distribution of the fraction of extracted Pb (%) for each extractant: distilled water (in black circles), humic acid (in white circles) and EDTA (in grey circles). The 3 extraction groups were distinguished according to the amount of extracted Pb with distilled water and EDTA, the Pb contamination (EF_{Pb}) and the proximity of the slag heap (see text).